Title
Modeling Elastic Waves in Fractured Rock with the Kirchhoff Method

Author
Nihei, K.T.

Publication Date
1989-11-01

LBL-30688

Lawrence Berkeley Laboratory
UNIVERSITY OF CALIFORNIA

EARTH SCIENCES DIVISION

Modeling Elastic Waves in Fractured Rock with the Kirchhoff Method

K.T. Nihei
(M.S. Thesis)

November 1989

Prepared for the U.S. Department of Energy under Contract Number DE-AC03-76SF00098

DISCLAIMER

LBL-30688

Modeling Elastic Waves in Fractured Rock with the Kirchhoff Method

Kurt Toshimi Nihei

(M.S. Thesis)

Department of Materials Science and Mineral Engineering
University of California

and

Earth Sciences Division
Lawrence Berkeley Laboratory
University of California
Berkeley, California 94720

November 1989

In addition to support from the Jane Lewis Fellowship, this work was supported by the Manager, Chicago Operations, Repository Technology Program, Repository Technology and Transportation Division, of the U.S. Department of Energy under Contract No. DE-AC03-76SF00098.

Modeling Elastic Waves in Fractured Rock with the Kirchhoff Method

Kurt Toshimi Nihei

Department of Materials Science and Mineral Engineering
University of California, Berkeley

Abstract

This study presents a numerical approach for modeling elastic wave propagation across single and multiple fractures. The approach is based on the Kirchhoff method. Fractures are modeled as infinitesimally thin, non-welded, rectangular contacts embedded in a homogeneous, isotropic medium. In this model, tractions are continuous and displacements are discontinuous across the fracture. The magnitude of the displacement discontinuity is equal to the ratio of the stress to the stiffness of the fracture.

The effects of a fracture on elastic waves are investigated by incorporating plane wave reflection and transmission coefficients for the fracture into the Kirchhoff method. Synthetic seismograms for the transmitted and reflected waves are generated for fractures with constant and random stiffness surfaces.

The numerical results show that a fracture produces converted waves and diffracted waves from the fracture edges. The amplitude and frequency content of these waves are controlled by the stiffness of the fracture and the angle of the incident plane wave. When the stiffness varies randomly along the surface of the fracture scattered waves are also generated.

Acknowledgements

I would like to thank Professors L. R. Johnson, N. G. W. Cook, and H. F. Morrison for their comments and criticisms; Clarence and Evelyn Nihei and Leigh Anne Yonago for their encouragement and support; and Dr. J. C. S. Long and Dr. Kenzi Karasaki for introducing me to some of the numerical aspects of fluid flow in fractured media. In addition to support from the Jane Lewis Fellowship, I wish to acknowledge the partial support of the Manager, Chicago Operations, Repository Technology Program, Repository Technology and Transportation Division of the U.S. Department of Energy under Contract No. DE-AC03-76SF00098.

Table of Contents

CHAPTER 1

INTRODUCTION

Interconnected fractures can serve as major conduits for fluid flow in the subsurface. A knowledge of the location, orientation, and permeability of fractures is therefore important for optimal geothermal and petroleum production as well as hazardous waste isolation.

Well logs and core samples can provide valuable information about the orientation and permeability of fractures near the well. However, the cost of drilling usually limits the number of wells, and in the context of waste isolation, the presence of wells may jeopardize the integrity of the site. Seismic techniques for characterizing fractures away from the well have been the subject of many recent studies. Seismic reflection (Palmer, 1982; Green and Mair, 1982), vertical seismic profiling (Stewart et. al., 1981; Majer et. al., 1988; Carswell and Moon, 1989), and crosshole tomography (Wong et. al., 1983; Majer et al., 1987) have been used to estimate the location, orientation, and density of fractures in crystalline rock and shale. Despite the success reported by many of these studies, the interaction of an elastic wave with a fracture is still an area of active research (Pyrak, 1988; Suarez et. al., 1988; Hardin et. al., 1987). A detailed understanding of this interaction may lead to more successful methods of fracture detection and characterization.

This study examines the effects of single and multiple, 3-dimensional fractures on elastic waves. Fractures are modeled as non-welded, rectangular surfaces with frequency and stiffness dependent reflection and transmission coefficients developed by Shoenberg (1980) and Pyrak (1988). The elastic wave displacements are calculated using the elastic Kirchhoff method. The amplitudes and the frequency content of the transmitted and reflected waves are also examined.

A description of the elastic Kirchhoff method and the fracture model along with their limitations are given in Chapter 2. Details necessary for the numerical implementation of the method are also presented. In Chapter 3, the accuracy of the elastic Kirchhoff method is tested by comparing numerical results with the free-space and half-space elastic Green's functions. Results for a single fracture and for two fractures are also presented. Summary and conclusions are given in Chapter 4.

1.1 Review of Previous Work

The interaction of an elastic wave with a fracture has been the subject of many experimental and theoretical studies. The purpose of these studies is to develop methods to locate and determine the orientation of fractures from seismic measurements.

Most seismic methods for characterizing fractured rock fall into two categories. The first category attempts to determine the bulk properties of a fractured rock mass such as the predominant fracture orientation and density of fractures by relating theoretical effective anisotropy relations for cracked solids (Crampin, 1981; Hudson, 1981) to observations of shear wave splitting, particle polarization anomalies, and directionally dependent velocities. Because of approximations made in the derivation of these relations, this is a quasi-static approach valid only for seismic wavelengths long in comparison with the dimensions of the cracks and for dilute concentrations of cracks (Chatterjee and Mal, 1978). The second category is concerned with locating discrete fractures or fractured zones that are large in comparison to the seismic wavelength from travel time, amplitude, and scattered wave observations. In this study, we will be concerned with the latter problem.

Green and Mair (1982) performed a high resolution surface reflection survey over crystalline rock. They observed strong reflections which they attributed to subhorizontal fracture zones with high acoustical impedances. Carswell and Moon (1989) analyzed multi-offset VSP data from a survey 12 km northeast of the surface reflection site and also observed reflected arrivals which they interpreted as evidence for extensive, subhorizontal fracture zones up to 6 m thick.

Stewart et. al. (1981) used VSP travel time measurements of P and SH waves made before and after an explosive fracturing of shale. From travel time delay, attenuation, and converted and scattered wave observations, they estimated the location, extent, shape, and porosity of the fractured zone. Wong et. al. (1983) and Majer et. al. (1987) applied ray tomography to crosshole travel time and amplitude measurements made in crystalline rock and obtained profiles of seismic velocity and attenuation that correlated well with fractured zones observed around the borehole.

Palmer (1982) investigated the application of reflected ultrasonic waves to detect fractures. Fractures where modeled as thin, planar layers filled with interstitial material (air, water, calcite, silica)

located within a granite slab. Reflected SH waves were found to be better for detecting fractures but both P and SH waves were needed to distinguish between water filled and air filled fractures.

Several promising crosshole studies were performed at the Fenton Hill Hot Dry Rock geothermal reservoir (Fehler and Pearson, 1984; Aki et. al. 1982; Fehler, 1982). These studies were aimed at determining whether or not large fluid-filled fractures were present between two boreholes. They used 4-15 kHz seismic waves and estimated the location and degree of fracturing based on observations of waveform character, decreases in signal amplitude, and reduction in the high frequency content of the wave.

Recent developments in seismic imaging methods using the scattered wavefield may emerge as valuable compliments to ray tomography and seismic reflection methods. Diffraction tomography (Wu and Toksoz, 1987; Pratt and Worthington, 1988) and Born inversion (LeBras and Clayton, 1988) are presently restricted to acoustic waves and weak scattering but there has been recent work to extend these methods to handle elastic waves and multiple scattering. These methods are attractive because they use information which is often excluded in conventional analyses of VSP and crosshole seismic measurements.

1.2 Preview of This Study

The success of seismic methods for fracture detection and characterization requires a detailed understanding of the interaction of an elastic wave with a fracture. In this study, the Kirchhoff method is used to numerically model elastic wave transmission and reflection from single and multiple fractures. Fractures are treated as a non-welded contacts across which the stress is continuous but the displacement is discontinuous. The magnitude of the displacement discontinuity is equal to the ratio of the stress to the stiffness of the fracture. The synthetic results generated with the Kirchhoff method show that the interaction of an elastic wave with a fracture produces a reduction in wave amplitude, a reduction in the high frequency content of the wave, converted waves, and diffracted waves from the fracture edges.

CHAPTER 2

ELASTIC KIRCHHOFF METHOD FOR FRACTURED ROCK

2.1 Introduction

For problems in seismology involving the reflection and transmission of waves at boundaries it is often convenient to work with the integral form of the elastodynamic equation. The advantage of using the integral representation of the seismic wavefield is that it does not require absorbing boundary conditions and extensive gridding of the entire medium that are necessary in finite difference and finite element methods. The drawback, however, is that a Green's function is needed to propagate waves between boundaries. In the case where the boundaries are separated by homogeneous material a free-space Green's function can be used. When the medium parameters are variable exact Green's functions are usually not available and asymptotic Green's functions must be constructed (Bleistein, 1986; Cohen, 1988).

The integral representation of a seismic wavefield can be viewed as a mathematical statement of Huygen's Principle for elastic waves (Baker and Copson, 1950; Pao and Mow, 1973; Pao and Varatharajulu, 1976). A wave incident upon a boundary surface gives rise to secondary point sources that emit both P and S waves. Summing the effects of these secondary sources located on the boundary surface at the receiver location produces constructive and destructive interference that defines transmitted, reflected, and diffracted waves (Figure 2.1).

The problem in evaluating the integral representation for the displacement at a point in the medium is that the displacements and tractions along the boundary appear in the integrand and, therefore, must be known a priori. The boundary integral equation method (BIEM) solves for these values by placing the receiver on the boundary, discretizing the boundary into nodal points, applying the boundary conditions, and solving the resulting system of linear equations (Cole, 1980; Schuster and Smith, 1985). Once the values of stress and displacement are known along the boundary for a particular source, the displacement can be evaluated at a receiver located anywhere in the medium. The problem with the BIEM approach is that for high frequency, 3-dimensional, elastic problems typically encoun-

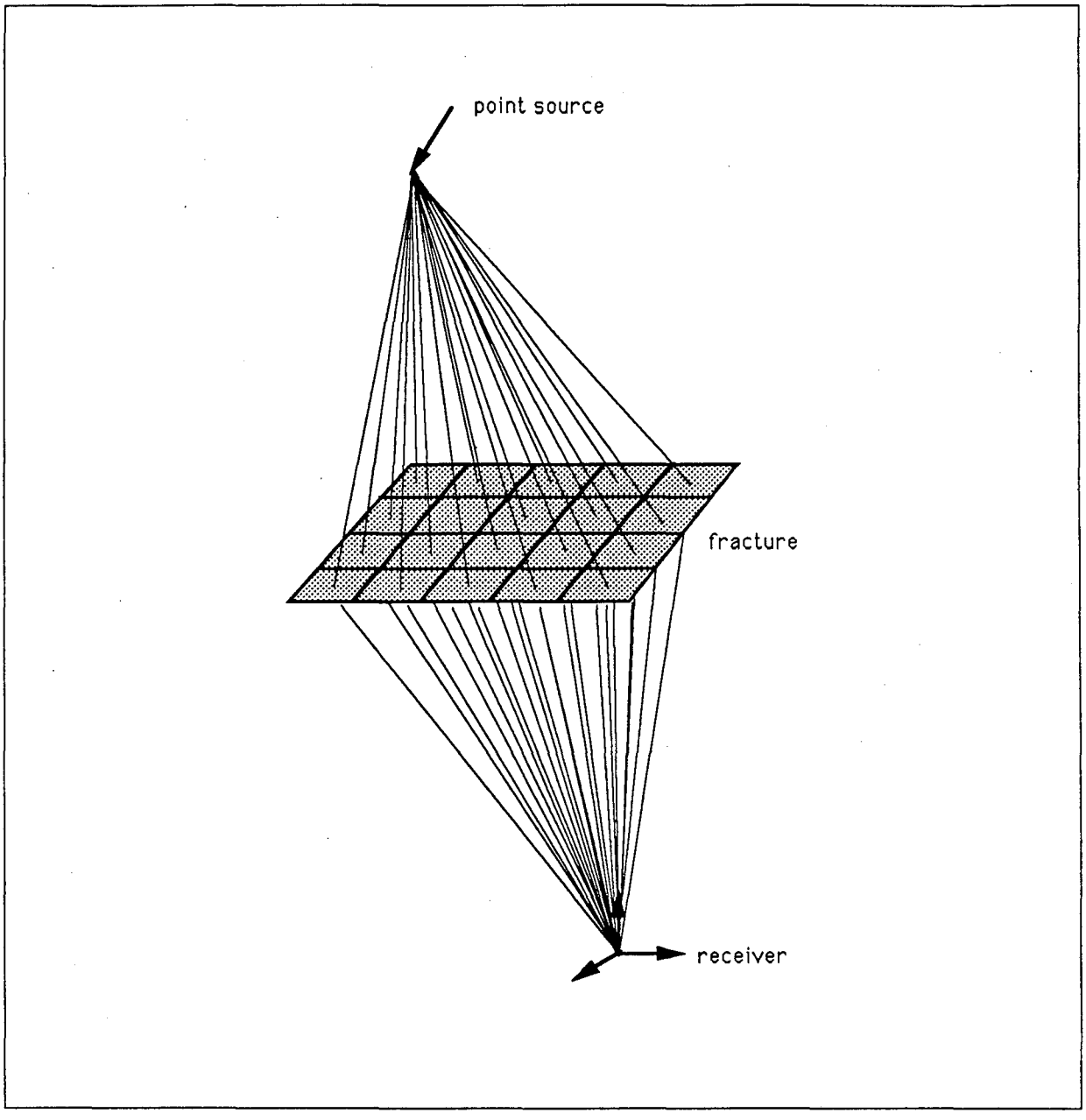

Figure 2.1 Conceptual description of the Kirchhoff Method.

tered in fracture studies it requires large matrix inversions that are computationally intensive.

A more feasible approach is to approximate the surface displacements and tractions using ray theory and plane wave reflection and transmission coefficients. This approach is called the Kirchhoff method. The Kirchhoff method has several advantages over geometric ray theory: it includes diffractions from surface irregularities and does not break down when the receiver is located on a caustic. In the geophysics literature, the Kirchhoff method has been used to model scattered acoustic waves (Trorey, 1970, 1977; Hilterman, 1970, 1975; Haddon and Buchen, 1981; Deregowski and Brown, 1983; Scott, 1985; Sullivan, 1987) and elastic waves (Frazer and Sen, 1985; Sen and Frazer, 1985, 1987; Frazer, 1987; Sumner, 1988).

In this study, we are interested in the effects of fractures or joints on elastic waves. A fracture is modeled as a non-welded contact across which traction is continuous and displacement is discontinous (Shoenberg, 1980). The magnitude of the displacement discontinuity is controlled by the ratio of the stress to the fracture stiffness. From these boundary conditions for traction and displacement across a fracture, frequency dependent plane wave transmission and reflection coefficients are derived. Converted and diffracted P and S waves from a fracture surface are modeled by incorporating reflection and transmission coefficients derived from this fracture model into the Kirchhoff method. Details of the Kirchhoff method and the displacement discontinuity fracture model are given in the following section.

2.2 Description of the Kirchhoff Method

The integral representation theorem for an elastic medium specifies the manner in which the displacement at an observation point is constructed from a surface integral over surface traction and displacement (Aki and Richards, 1980). It has been used extensively to model earthquake source processes (Dmonska and Rice, 1983) and scattering from obstacles (Pao and Mow, 1973). The elastic Kirchhoff method provides an approximate solution of the integral representation theorem through the use of the Kirchhoff approximation.

2.2.1 Integral Representation Theorem

To obtain the integral representation theorem, first consider the displacement and stress fields on the surface, S, produced by a body force located inside the volume, V, at a point $\mathbf{r}_s$ (Figure 2.2). The corresponding equation of motion for a Cartesian coordinate system is

$$\nabla\cdot\tau_1(\mathbf{r}',t) + \mathbf{f}_1(\mathbf{r}_s,t) = \rho\frac{\partial^2}{\partial^2 t}\mathbf{u}_1(\mathbf{r}',t) \tag{2.1a}$$

where $\mathbf{u}_1$ is the displacement, ρ is the density, $\mathbf{f}_1$ is the body force density causing the disturbance, τ_1 is the stress tensor, t is the time, and $\mathbf{r}'=(x',y',z')$ and $\mathbf{r}_s=(x_s,y_s,z_s)$ are position vectors shown in Figure 2.2. Similarly, consider the displacement and stress fields on S due to a body force located inside V at a point $\mathbf{r}$. The equation of motion is

$$\nabla\cdot\tau_2(\mathbf{r}',t) + \mathbf{f}_2(\mathbf{r},t) = \rho\frac{\partial^2}{\partial^2 t}\mathbf{u}_2(\mathbf{r}',t) \tag{2.1b}$$

In both equations (2.1a,b), V is taken to be large so that the displacements and tractions on S_b, the surface bounding V, are negligible.

It is convenient to work in the frequency domain when any material parameters are frequency dependent. The Fourier transform and its inverse are defined by

$$\hat{g}(\omega) = \int_{-\infty}^{\infty} g(t)e^{-i\omega t}\,dt \tag{2.2}$$

$$g(t) = \frac{1}{2\pi}\int_{-\infty}^{\infty} \hat{g}(\omega)e^{i\omega t}\,d\omega$$

Taking the Fourier transform of equations (2.1a) and (2.1b) gives two time transformed equations of motion.

$$\nabla\cdot\tau_1(\mathbf{r}',\omega) + \mathbf{f}_1(\mathbf{r}_s,\omega) = -\rho\omega^2\mathbf{u}_1(\mathbf{r}',\omega) \tag{2.3a}$$

$$\nabla\cdot\tau_2(\mathbf{r}',\omega) + \mathbf{f}_2(\mathbf{r},\omega) = -\rho\omega^2\mathbf{u}_2(\mathbf{r}',\omega) \tag{2.3b}$$

where the $\hat{}$ symbol will be suppressed, henceforth, so that $\mathbf{u}$, τ, and $\mathbf{f}$ imply the Fourier transformed values. Multiplying equation (2.3a) by $\mathbf{u}_2$ and equation (2.3b) by $\mathbf{u}_1$ and subtracting the resulting equations gives

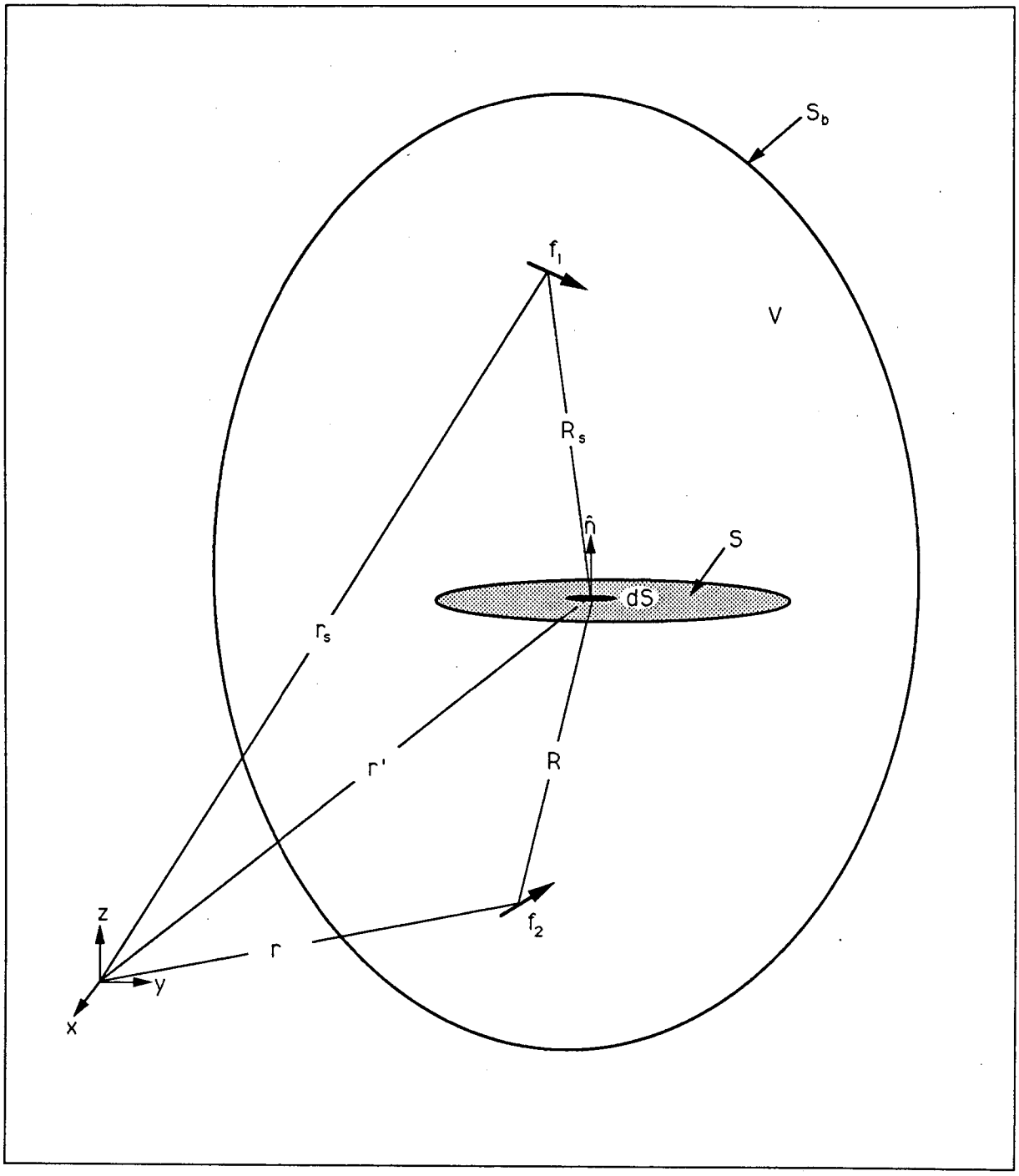

Figure 2.2 Problem geometry used in the derivation and evaluation of the integral representation theorem.

$$[\nabla\cdot\boldsymbol{\tau}_1(\mathbf{r}',\omega)]\cdot\mathbf{u}_2(\mathbf{r}',\omega) - [\nabla\cdot\boldsymbol{\tau}_2(\mathbf{r}',\omega)]\cdot\mathbf{u}_1(\mathbf{r}',\omega) = -\mathbf{f}_1(\mathbf{r}_s,\omega)\cdot\mathbf{u}_2(\mathbf{r}',\omega) + \mathbf{f}_2(\mathbf{r},\omega)\cdot\mathbf{u}_1(\mathbf{r}',\omega) \tag{2.4}$$

The two terms on the left hand side can be further simplified by the following identity valid for any vector $\mathbf{u}$ and second order tensor $\boldsymbol{\tau}$ (Frazer and Sen, 1985): $\nabla\cdot(\boldsymbol{\tau}\cdot\mathbf{u}) = (\nabla\cdot\boldsymbol{\tau})\mathbf{u} - \boldsymbol{\tau}:\nabla\mathbf{u}$

$$\begin{aligned}\nabla\cdot[\boldsymbol{\tau}_1(\mathbf{r}',\omega)\cdot\mathbf{u}_2(\mathbf{r}',\omega) - \boldsymbol{\tau}_2(\mathbf{r}',\omega)\cdot\mathbf{u}_1(\mathbf{r}',\omega)] - \boldsymbol{\tau}_1(\mathbf{r}',\omega):\nabla\mathbf{u}_2(\mathbf{r}',\omega) + \boldsymbol{\tau}_2(\mathbf{r}',\omega):\nabla\mathbf{u}_1(\mathbf{r}',\omega) \\ = [\mathbf{f}_2(\mathbf{r},\omega)\cdot\mathbf{u}_1(\mathbf{r}',\omega) - \mathbf{f}_1(\mathbf{r}_s,\omega)\cdot\mathbf{u}_2(\mathbf{r}',\omega)]\end{aligned} \tag{2.5}$$

The third and forth terms on the left hand side of equation (2.5) cancel because of the symmetries of the fourth order elastic tensor, $\mathbf{c}$ (Frazer and Sen, 1985).

$$\boldsymbol{\tau}_1:\nabla\mathbf{u}_2 = (\mathbf{c}:\nabla\mathbf{u}_1):\nabla\mathbf{u}_2 = \nabla\mathbf{u}_1:\mathbf{c}:\nabla\mathbf{u}_2 = \nabla\mathbf{u}_2:\mathbf{c}:\nabla\mathbf{u}_1 = \boldsymbol{\tau}_2:\nabla\mathbf{u}_1$$

Integrating both sides of equation (2.5) over V gives

$$\int_V \nabla\cdot[\boldsymbol{\tau}_1(\mathbf{r}',\omega)\cdot\mathbf{u}_2(\mathbf{r}',\omega) - \boldsymbol{\tau}_2(\mathbf{r}',\omega)\cdot\mathbf{u}_1(\mathbf{r}',\omega)]\,dV = \int_V [\mathbf{f}_2(\mathbf{r},\omega)\cdot\mathbf{u}_1(\mathbf{r}',\omega) - \mathbf{f}_1(\mathbf{r}_s,\omega)\cdot\mathbf{u}_2(\mathbf{r}',\omega)]\,dV \tag{2.6}$$

For a volume, V, bounded by a closed surface, S_b, within which $\boldsymbol{\tau}$ and $\mathbf{u}$ are analytic functions, the integral on the left hand side can be converted from a volume integral to a surface integral through an application of the divergence theorem

$$\int_S [\boldsymbol{\tau}_1(\mathbf{r}',\omega)\cdot\mathbf{u}_2(\mathbf{r}',\omega) - \boldsymbol{\tau}_2(\mathbf{r}',\omega)\cdot\mathbf{u}_1(\mathbf{r}',\omega)]\cdot\hat{n}\,dS = \int_V [\mathbf{f}_2(\mathbf{r},\omega)\cdot\mathbf{u}_1(\mathbf{r}',\omega) - \mathbf{f}_1(\mathbf{r}_s,\omega)\cdot\mathbf{u}_2(\mathbf{r}',\omega)]\,dV \tag{2.7}$$

where $\hat{n}$ is the outer normal to a surface element, dS. Equation (2.7) is a general relation between the displacements and tractions produced by a pair of body forces (Aki and Richards, 1980).

An integral representation theorem that describes the displacement at $\mathbf{r}$ can be obtained directly from this relation if the displacement, $\mathbf{u}_2$, and stress, $\boldsymbol{\tau}_2$, are known. If we assume that the body force density at $\mathbf{r}$ is a point force, $\mathbf{f}_2(\mathbf{r},\omega) = \delta(x-x')\delta(y-y')\delta(z-z') = \delta(\mathbf{r}-\mathbf{r}')$, then

$$\mathbf{u}_2(\mathbf{r}',\omega) = \mathbf{G}(\mathbf{r}'|\mathbf{r},\omega) = \mathbf{G}(\mathbf{r}|\mathbf{r}',\omega) \tag{2.8a}$$

$$\boldsymbol{\tau}_2(\mathbf{r}',\omega) = \boldsymbol{\Sigma}(\mathbf{r}'|\mathbf{r},\omega) = \boldsymbol{\Sigma}(\mathbf{r}|\mathbf{r}',\omega) \tag{2.8b}$$

where δ is the Dirac delta function, $\mathbf{G}$ is the Green's function, and $\boldsymbol{\Sigma}$ is the third rank Green's stress tensor. Physically, $\mathbf{G}$ and $\boldsymbol{\Sigma}$ represent the displacement and stress fields at $\mathbf{r}$ produced by three mutually perpendicular concentrated point forces located at $\mathbf{r}'$ (Pao and Varatharajulu, 1976). In the exam-

ples presented in the following chapter, it is assumed that the medium is homogeneous and isotropic. The time transformed free-space Green's displacement dyadic and Green's stress tensor in a Cartesian coordinate system are given in indicial notation by (Kuo and Dai, 1984)

$$G_{mn} = \frac{1}{4\pi\rho\omega^2}\left[\frac{\delta_{mn}}{R^2}(1 - ik_\alpha R) - \frac{\gamma_m\gamma_n}{R^2}(3 - 3ik_\alpha R - k_\alpha{}^2R^2)\right]\frac{e^{ik_\alpha R}}{R} + \frac{1}{4\pi\rho\omega^2}\left[\frac{-\delta_{mn}}{R^2}(1 - ik_\beta R - k_\beta{}^2R^2) + \frac{\gamma_m\gamma_n}{R^2}(3 - 3ik_\beta R - k_\beta{}^2R^2)\right]\frac{e^{ik_\beta R}}{R} \tag{2.9}$$

$$\Sigma_{lmn} = \lambda\delta_{lm}\frac{\partial G^\alpha_{kn}}{\partial x_k} + \mu\left[\frac{\partial G^\alpha_{mn}}{\partial x_l} + \frac{\partial G^\alpha_{ln}}{\partial x_m}\right] + \mu\left[\frac{\partial G^\beta_{mn}}{\partial x_l} + \frac{\partial G^\beta_{ln}}{\partial x_m}\right] \tag{2.10}$$

where R is the distance from the surface to the receiver, and $k_\alpha=\omega/\alpha$ and $k_\beta=\omega/\beta$ are the wavenumbers for P and S waves.

Inserting the expressions for $\mathbf{u}_2$ and τ_2 given in equations (2.8a-b) into the relation (2.7) results in the following equation.

$$\int_S [\tau_1(\mathbf{r}',\omega)\cdot\mathbf{G}(\mathbf{r}|\mathbf{r}',\omega) - \Sigma(\mathbf{r}|\mathbf{r}',\omega)\cdot\mathbf{u}_1(\mathbf{r}',\omega)]\cdot\hat{n}\ dS = \int_V \delta(\mathbf{r}-\mathbf{r}')\cdot\mathbf{u}_1(\mathbf{r}',\omega)\ dV - \int_V \mathbf{f}_1(\mathbf{r}_s,\omega)\cdot\mathbf{G}(\mathbf{r}|\mathbf{r}',\omega)\ dV \tag{2.11}$$

The first integral on the right hand side can be simplified using the sifting property of the Dirac delta function: $\int_V \delta(\mathbf{r}-\mathbf{r}')\cdot\mathbf{u}_1(\mathbf{r}',\omega)dV=\mathbf{u}_1(\mathbf{r},\omega)$.

$$\mathbf{u}_1(\mathbf{r},\omega) = \int_V \mathbf{f}_1(\mathbf{r}_s,\omega)\cdot\mathbf{G}(\mathbf{r}|\mathbf{r}',\omega)\ dV + \int_S [\hat{n}\cdot\tau_1(\mathbf{r}',\omega)\cdot\mathbf{G}(\mathbf{r}|\mathbf{r}',\omega) - \hat{n}\cdot\Sigma(\mathbf{r}|\mathbf{r}',\omega)\cdot\mathbf{u}_1(\mathbf{r}',\omega)]\ dS \tag{2.12}$$

Equation (2.12) describes the displacement at $\mathbf{r}$ produced by a body force located at $\mathbf{r}_s$. The first integral describes waves traveling directly from the source, $\mathbf{f}_1$, to a receiver located at $\mathbf{r}$. The second integral contains the effects of the surface displacements and tractions on S produced by $\mathbf{f}_1$ and can be viewed as the scattered wavefield contribution. Since we are interested in the portion of the wavefield that has interacted with the surface, S, we can drop the first integral in equation (2.12) that corresponds to the direct wave.

$$\mathbf{u}(\mathbf{r},\omega) = \int_S [\hat{n}\cdot\tau(\mathbf{r}',\omega)\cdot\mathbf{G}(\mathbf{r}|\mathbf{r}',\omega) - \hat{n}\cdot\Sigma(\mathbf{r}|\mathbf{r}',\omega)\cdot\mathbf{u}(\mathbf{r}',\omega)]\ dS \tag{2.13}$$

The subscript 1 has been dropped since it is understood that the wavefield originates from the body force density, $\mathbf{f}_1$.

Equation (2.13) is the integral representation theorem or elastic Kirchhoff integral. The integral representation theorem is formally stated for a closed surface. It can be used to calculate the response of a finite surface, S, by constructing a spherical surface, S' , of large radius (Figure 2.3). The contributions from S' arrive much later in time than the contributions from S and can be neglected in the evaluation of the integral. This follows directly from a consideration of the Sommerfeld radiation condition for elastic waves (Achenbach, 1982).

2.2.2 Reduction to a 2.5D Problem

Equation (2.13) can be reduced from a surface integral to a line integral if the source and receiver are located in a plane perpendicular (P and SV waves only) or parallel (SH waves only) to the direction in which the material properties are uniform. This problem geometry is called 2.5D because the medium properties vary in only two directions while the source produces three dimensional waves (Bleistein, 1986). Figure 2.4 shows the 2.5D problem geometry for P and SV waves. The motivation for reducing the 3D problem to a 2.5D problem is the significant reduction in the computation time needed for the numerical evaluation the the Kirchhoff integral.

To reduce equation (2.13) to a line integral, the x-dependence is integrated out using the method of stationary phase (Bleistein, 1982) or the method of steepest descent (Aki and Richards, 1980; Bleistein, 1982; Achenbach et. al., 1982). The method of stationary phase is used in the following derivation of the 2.5D Kirchhoff integral. Starting with equation (2.13)

$$\mathbf{u}(\mathbf{r},\omega) = \int_S [\hat{n}\cdot\boldsymbol{\tau}(\mathbf{r}',\omega)\cdot\mathbf{G}(\mathbf{r}|\mathbf{r}',\omega) - \hat{n}\cdot\boldsymbol{\Sigma}(\mathbf{r}|\mathbf{r}',\omega)\cdot\mathbf{u}(\mathbf{r}',\omega)]\, dS$$

note that dS can be described by the following equation.

$$dS = \left[1 + \left[\frac{\partial z}{\partial x}\right]^2 + \left[\frac{\partial z}{\partial y}\right]^2\right]^{1/2} dx\ dy \qquad (2.14)$$

$$= D(x,y)\ dx\ dy$$

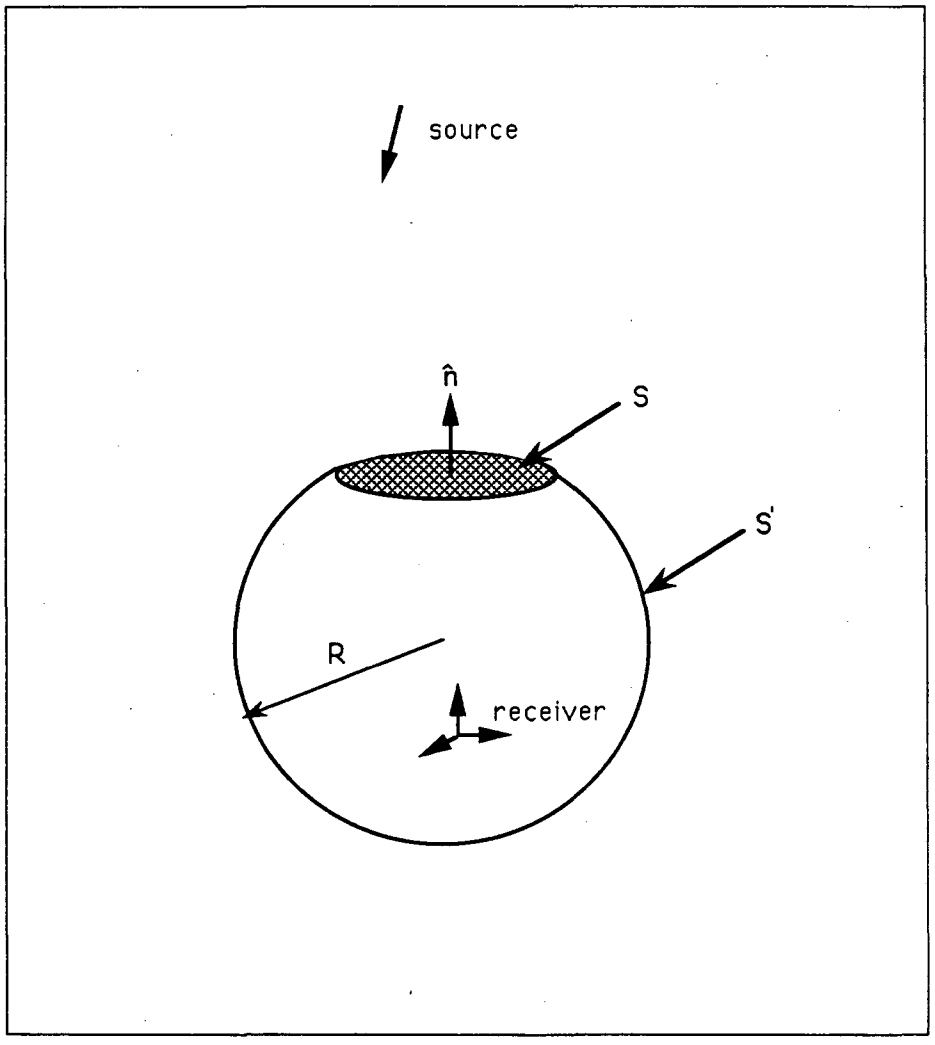

Figure 2.3 Closed surface of integration used in the evaluation of the Kirchhoff integral. As R goes to infinity, the S' contribution in the integral goes to zero.

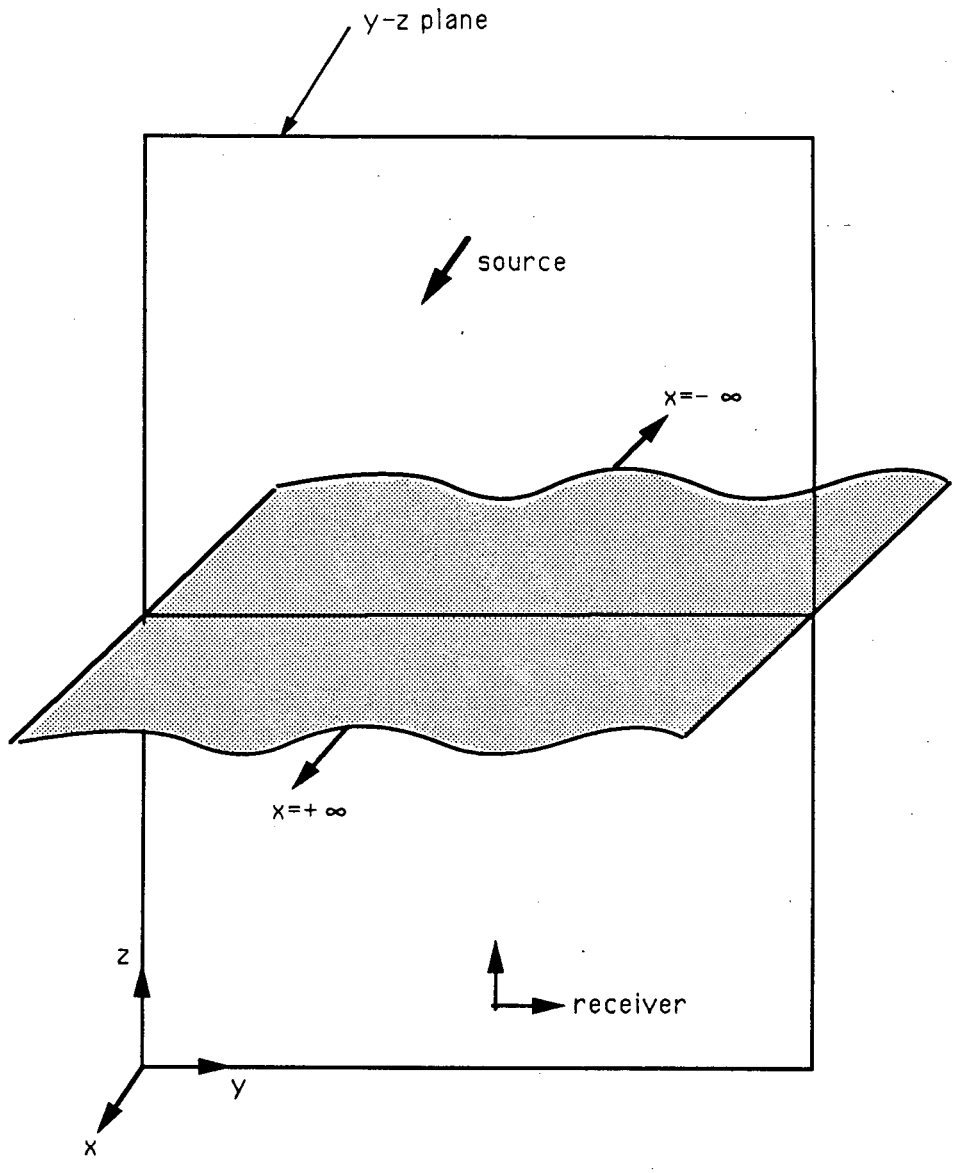

Figure 2.4 Geometry for the 2.5D problem. Source and receiver are located in the y-z plane and the surface properties are constant in the x-direction.

Upon substitution of equation (2.14), equation (2.13) becomes

$$\mathbf{u}(\mathbf{r},\omega) = \iint \left\{ D(x,y)\,[\hat{n}\cdot\boldsymbol{\tau}\cdot\mathbf{G} - \hat{n}\cdot\boldsymbol{\Sigma}\cdot\mathbf{u}] \right\} dx\ dy \tag{2.15}$$

Substituting the expressions for $\boldsymbol{\tau}$, $\mathbf{G}$, $\mathbf{u}$, and $\boldsymbol{\Sigma}$ given in the previous section into equation (2.15) results in an oscillatory integral of the form

$$\mathbf{u}(\mathbf{r},\omega) = \iint E(x,y)\, e^{[i\omega\phi(x,y)]}\, dx\ dy \tag{2.16}$$

where $E(x,y)$ contains the non-exponential terms and $\phi(x,y)$ is the phase given by

$$\phi(x,y) = \left[\frac{R_s}{c_s} + \frac{R}{c} \right] \tag{2.17}$$

where R_s and R are the distances from the source to the surface and the surface to the receiver, respectively, and c_s and c are the velocities of the waves traveling from the source to the surface and the surface to the receiver, respectively.

Both $E(x,y)$ and $\phi(x,y)$ are assumed to be independent of ω and analytic functions of x . When ω is large, rapid oscillations of the phase result in positive and negative contributions to the integral that tend to cancel, making $\mathbf{u}(\mathbf{r},\omega)$ small. The major contributions to the integral occur where the phase is stationary or where there are discontinuities in $E(x,y)$ or $\phi(x,y)$. The former contribution produces specular reflections and the latter, diffracted waves.

To evaluate equation (2.16) by the method of stationary phase, an expansion of the phase is made about the stationary point, x_{sp} .

$$\phi(x,y) \approx \phi(x_{sp},y) + (x-x_{sp})\phi'(x_{sp},y) + \frac{(x-x_{sp})^2}{2}\phi''(x_{sp},y) + O^3(x_{sp},y) \tag{2.18}$$

Here, the $'$ symbol is used to denote the partial derivative, $\partial/\partial x$. Substituting equation (2.18) into equation (2.16) and neglecting the higher order terms gives

$$\mathbf{u}(\mathbf{r},\omega) \approx \iint E(x,y)\, \exp\left\{ i\omega \left[\phi(x_{sp},y) + \frac{(x-x_{sp})^2}{2}\phi''(x_{sp},y) \right] \right\} dx\ dy$$

$$= \int \exp[i\omega\phi(x_{sp},y)] \int E(x,y)\, \exp\left[i\omega \frac{(x-x_{sp})^2}{2}\phi''(x_{sp},y) \right] dx\ dy \tag{2.19}$$

Making the following substitution for the exponential term in the second integral

$$\chi^2 = \frac{(x-x_{sp})^2}{2}\phi''(x_{sp},y) \tag{2.20}$$

simplifies equation (2.19)

$$\mathbf{u}(\mathbf{r},\omega) = \int \exp[i\,\omega\phi(x_{sp},y)] \int F(\chi,y)\,\exp[i\,\omega\chi^2]\,d\chi\,dy \tag{2.21}$$

where $F(\chi,y) = E(x,y)\,dx/d\chi$. The procedure for obtaining an asymptotic solution of the second integral in equation (2.21) is given by Bleistein (1982). For brevity, only the result is given below.

$$\int F(\chi,y)\,\exp[i\,\omega\chi^2]\,d\chi \approx \left[\frac{2\pi}{\omega\phi''(x_{sp},y)}\right]^{1/2} E(x_{sp},y)\,e^{i\frac{\pi}{4}} \tag{2.22}$$

Through a substitution of equation (2.22), equation (2.21) simplifies to a single integral over y.

$$\mathbf{u}(\mathbf{r},\omega) = \left[\frac{2\pi}{\omega}\right]^{1/2} e^{i\pi/4} \int [\phi''(x_{sp},y)]^{-1/2}\,E(x_{sp},y)\,\exp[i\,\omega\phi(x_{sp},y)]\,dy \tag{2.23}$$

The stationary point, x_{sp}, is obtained by taking the partial derivative of the phase and setting it equal to zero.

$$\phi'(x_{sp},y) = x_{sp}\left[\frac{1}{c_s R_s} + \frac{1}{cR}\right] = 0 \tag{2.24}$$

From equation (2.24) it is clear that the stationary point is at $x_{sp} = 0$. The second derivative of the phase is

$$\phi''(x_{sp},y) = \left[\frac{1}{c_s R_s} + \frac{1}{cR}\right] \tag{2.25}$$

Substituting the values for x_{sp} and $\phi''(x_{sp},y)$ into equation (2.23) gives

$$\mathbf{u}(\mathbf{r},\omega) = \left[\frac{2\pi}{\omega}\right]^{1/2} e^{i\pi/4} \int \left[\frac{cRc_sR_s}{cR + c_sR_s}\right]^{1/2} E(0,y)\,e^{i\omega\phi(0,y)}\,dy \tag{2.26}$$

Equations (2.15) and (2.16) can be used to rewrite the last term in equation (2.26).

$$E(0,y)\,e^{i\omega\phi(0,y)} = D(0,y)\,[\hat{n}\cdot\boldsymbol{\tau}\cdot\mathbf{G} - \hat{n}\cdot\boldsymbol{\Sigma}\cdot\mathbf{u}]_{x_{sp}=0} \tag{2.27}$$

Substituting equation (2.27) into (2.26) results in the 2.5D Kirchhoff integral valid for high frequency waves

$$\mathbf{u}(\mathbf{r},\omega) = \left[\frac{2\pi}{\omega}\right]^{1/2} e^{i\pi/4} \int \left[\frac{cRc_s R_s}{c_s R_s + Rc}\right]^{1/2} \left[1 + \left[\frac{\partial z}{\partial y}^2\right]\right]^{1/2} [\hat{n}\cdot\boldsymbol{\tau}\cdot\mathbf{G} - \hat{n}\cdot\boldsymbol{\Sigma}\cdot\mathbf{u}]_{x_{sp}=0}\, dy \qquad (2.28)$$

where the subscript x_{sp}=0 denotes evaluation of $\mathbf{u}$, $\boldsymbol{\tau}$, $\mathbf{G}$, and $\boldsymbol{\Sigma}$ at the stationary point. The 2.5D Kirchhoff integral given in equation (2.28) is similar to the 3D Kirchhoff integral given in equation (2.13) except that the former has been reduced to a line integral with additional multiplier terms.

2.2.3 Kirchhoff Approximation

In this section, the Kirchhoff or tangent plane approximation is used to simplify the solution of the Kirchhoff integral. This approximation is based on the assumption that the incident wave is of sufficiently high frequency (i.e., the wavelength is much smaller than the correlation distance of any variation in material properties) that locally its amplitude decay is described by geometric ray theory and plane wave reflection and transmission coefficients (Scott, 1985). The Kirchhoff approximation has the following implications: (1) that every point on the surface of material discontinuity reflects the incident wave as though there were an infinite plane tangent to the surface at that point, and (2) that the values of displacement and traction at a point are independent of the boundary values at other points. This independence of displacement and traction between neighboring elements suggests that head waves, interface waves, and multiply scattered waves will not be included in Kirchhoff method solution.

Application of the Kirchhoff approximation to the 3D and 2.5D Kirchhoff integrals (equations (2.13) and (2.28), respectively) results in the following integrals for elastic wave transmission for a 3D problem geometry

$$\begin{aligned} u_n(\mathbf{r},\omega) = \int_S \Big\{ & T^{pp}[\hat{n}_l \tau^p_{lm} G^{\alpha}_{mn} - u^p_m(\hat{n}_l \Sigma^{\alpha}_{lmn})] + T^{ss}[\hat{n}_l \tau^{sv}_{lm} G^{\beta}_{mn} - u^{sv}_m(\hat{n}_l \Sigma^{\beta}_{lmn})] \\ & + T^{ps}[\hat{n}_l \tau^p_{lm} G^{\beta}_{mn} - u^p_m(\hat{n}_l \Sigma^{\beta}_{lmn})] + T^{sp}[\hat{n}_l \tau^{sv}_{lm} G^{\alpha}_{mn} - u^{sv}_m(\hat{n}_l \Sigma^{\alpha}_{lmn})] \\ & + T^{sh}[\hat{n}_l \tau^{sh}_{lm} G^{\beta}_{mn} - u^{sh}_m(\hat{n}_l \Sigma^{\beta}_{lmn})] \Big\}\, dS \end{aligned} \qquad (2.29a)$$

and for a 2.5D problem geometry

$$u_n(\mathbf{r},\omega) = \left[\frac{2\pi}{\omega}\right]^{1/2} e^{i\pi/4} \int \left[1 + \left[\frac{\partial z}{\partial y}^2\right]\right]^{1/2} \tag{2.29b}$$

$$\left\{ T^{pp} \left[\frac{\alpha R R_s}{R_s + R}\right]^{1/2} [\hat{n}_l \tau^p_{lm} G^{\alpha}_{mn} - u^p_m(\hat{n}_l \Sigma^{\alpha}_{lmn})]_{x_{sp}=0} \right.$$

$$+ T^{ps} \left[\frac{\beta R\, \alpha R_s}{\alpha R_s + \beta R}\right]^{1/2} [\hat{n}_l \tau^p_{lm} G^{\beta}_{mn} - u^p_m(\hat{n}_l \Sigma^{\beta}_{lmn})]_{x_{sp}=0}$$

$$+ T^{ss} \left[\frac{\beta R R_s}{R_s + R}\right]^{1/2} [\hat{n}_l \tau^{sv}_{lm} G^{\beta}_{mn} - u^{sv}_m(\hat{n}_l \Sigma^{\beta}_{lmn})]_{x_{sp}=0}$$

$$+ T^{sp} \left[\frac{\alpha R\, \beta R_s}{\beta R_s + \alpha R}\right]^{1/2} [\hat{n}_l \tau^{sv}_{lm} G^{\alpha}_{mn} - u^{sv}_m(\hat{n}_l \Sigma^{\alpha}_{lmn})]_{x_{sp}=0}$$

$$\left. + T^{sh} \left[\frac{\beta R R_s}{R_s + R}\right]^{1/2} [\hat{n}_l \tau^{sh}_{lm} G^{\beta}_{mn} - u^{sh}_m(\hat{n}_l \Sigma^{\beta}_{lmn})]_{x_{sp}=0} \right\} dy$$

where T^{pp} and T^{ps} are the plane wave transmission coefficients for an incident P wave; T^{ss} and T^{sp} are the transmission coefficients for an incident SV wave; and T^{sh} is the transmission coefficient for an incident SH wave. The reflected field is computed from the same equations by replacing the transmission coefficients with reflection coefficients.

The expressions for the displacements on the surface, S, are obtained from geometric ray theory. For a homogeneous, isotropic, elastic medium, the displacements on S are

$$u^p_m(\mathbf{r}',\omega) = \frac{1}{4\pi\rho R_s \alpha^2} [\gamma^p_m F^p_m(\omega) e^{i\omega t^{\alpha}}]$$

$$u^{sv}_m(\mathbf{r}',\omega) = \frac{1}{4\pi\rho R_s \beta^2} [\gamma^{sv}_m F^{sv}_m(\omega) e^{i\omega t^{\beta}}] \tag{2.30}$$

$$u^{sh}_m(\mathbf{r}',\omega) = \frac{1}{4\pi\rho R_s \beta^2} [\gamma^{sh}_m F^{sh}_m(\omega) e^{i\omega t^{\beta}}]$$

where $\mathbf{r}'$ is the position vector of the surface element, dS; R_s is the distance from the surface element to the receiver; γ^p_m, γ^{sv}_m, γ^{sh}_m are the direction cosines that define the $\hat{\mathbf{R}}_s$, $\hat{\mathbf{SH}}$, and $\hat{\mathbf{SV}}$ particle motions (see Figure 2.5);

$$\hat{\mathbf{R}}_s = \frac{\mathbf{R}_s}{|\mathbf{R}_s|} = \gamma^p_m \hat{\mathbf{x}}_m$$

$$\hat{\mathbf{SH}} = \frac{\hat{\mathbf{n}} \times (-\hat{\mathbf{R}}_s)}{\sin\theta} = \gamma^{sh}_m \hat{\mathbf{x}}_m \tag{2.31}$$

$$\hat{\mathbf{SV}} = \hat{\mathbf{SH}} \times \hat{\mathbf{R}}_s = \gamma^{sv}_m \hat{\mathbf{x}}_m$$

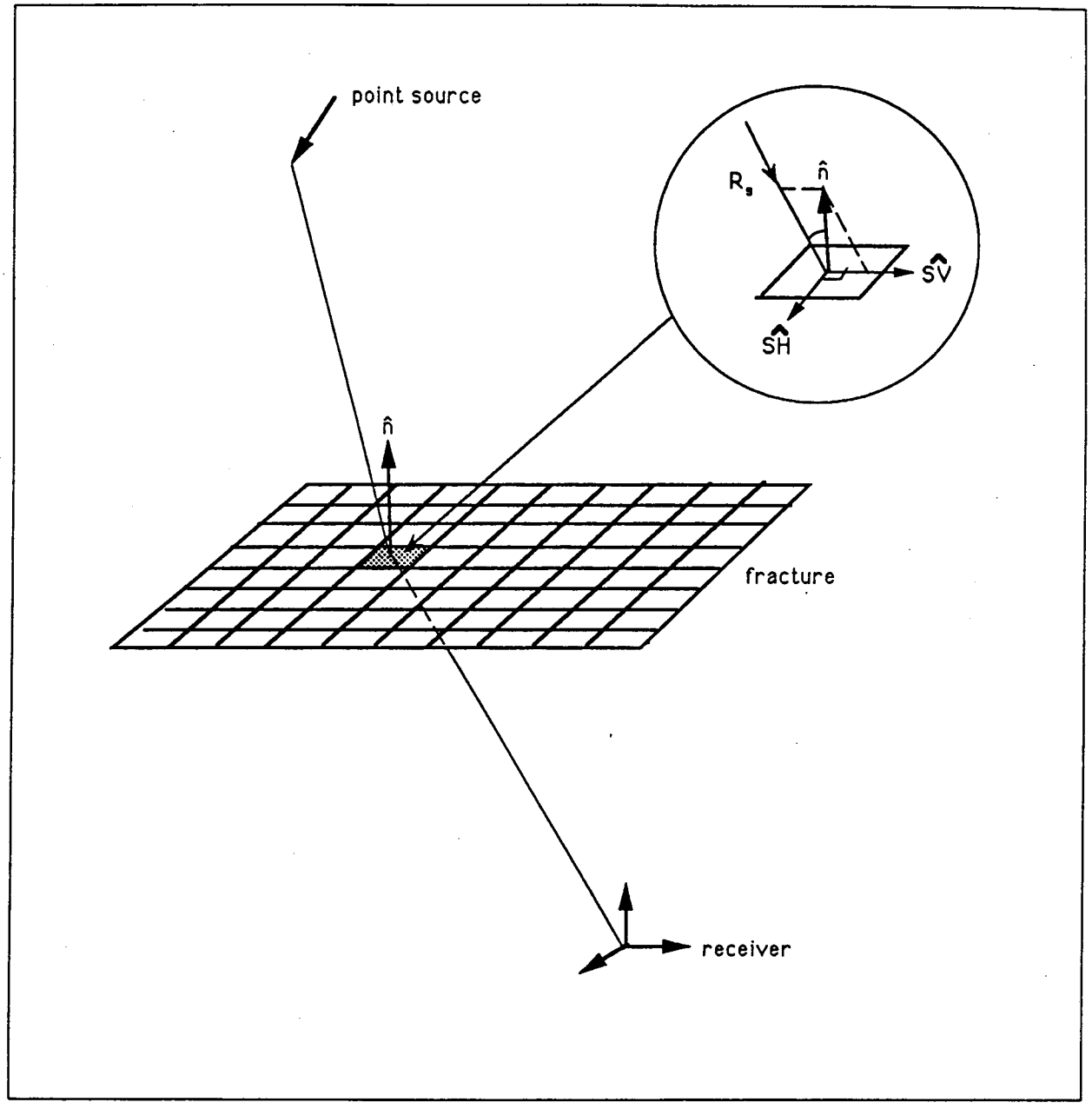

Figure 2.5 Vectors describing the particle motions of the P, SV, and SH waves on the fracture surface.

$F_m(\omega)$ is the source term; and $t^\alpha = R/\alpha$, and $t^\beta = R/\beta$ are the P and S wave travel times from the surface to the receiver. For a point source with source spectrum, $s(\omega)$, the source term is (Frazer and Sen, 1985)

$$\begin{aligned} F_m^p(\omega) &= \mathbf{s}(\omega) \cdot \hat{\mathbf{R}}_s = |s(\omega)|\gamma_m^{pt}\gamma_m^p \\ F_m^{sv}(\omega) &= \mathbf{s}(\omega) \cdot \hat{\mathbf{SV}} = |s(\omega)|\gamma_m^{pt}\gamma_m^{sv} \\ F_m^{sh}(\omega) &= \mathbf{s}(\omega) \cdot \hat{\mathbf{SH}} = |s(\omega)|\gamma_m^{pt}\gamma_m^{sh} \end{aligned} \tag{2.32}$$

where $\boldsymbol{\gamma}^{pt}$ are the direction cosines describing the orientation of the point force. General sources prescribed by their moment tensors (Aki and Richards, 1980) can be used in place of equation (2.32). However, a point force will be used to generate the synthetic waveforms in the next chapter so equation (2.32) will suffice.

The P and S wave stress tensors for an isotropic medium are

$$\tau_{lm}^p = \lambda \frac{\partial u_k^p}{\partial x_k}\delta_{lm} + \mu\left[\frac{\partial u_l^p}{\partial x_m} + \frac{\partial u_m^p}{\partial x_l}\right] \tag{2.33a}$$

$$\tau_{lm}^{sv} = \mu\left[\frac{\partial u_l^{sv}}{\partial x_m} + \frac{\partial u_m^{sv}}{\partial x_l}\right] \tag{2.33b}$$

$$\tau_{lm}^{sh} = \mu\left[\frac{\partial u_l^{sh}}{\partial x_m} + \frac{\partial u_m^{sh}}{\partial x_l}\right] \tag{2.33c}$$

For a plane wave propagating in the $\hat{\mathbf{k}}$ -direction, the displacement and its spatial derivative are

$$u_l = Ae^{-i(k_m x_m)} \tag{2.34a}$$

$$\frac{\partial u_l}{\partial x_m} = -ik_m Ae^{-i(k_m x_m)} = -\frac{i\omega}{c}\gamma_m^p u_l \tag{2.34b}$$

where A is the amplitude of the wave and $c = \alpha$, or β are the P wave and S wave velocities. Substitution of equation (2.34b) into equations (2.33a-c) gives the far-field approximation of the stress tensor.

$$\tau_{lm}^p = -\frac{i\omega}{\alpha}[\lambda\gamma_k^p u_k^p\delta_{lm} + \mu(\gamma_m^p u_l^p + \gamma_l^p u_m^p)] \tag{2.35a}$$

$$\tau_{lm}^{sv} = -\frac{i\omega\mu}{\beta}(\gamma_m^p u_l^{sv} + \gamma_l^p u_m^{sv}) \tag{2.35b}$$

$$\tau_{lm}^{sh} = -\frac{i\omega\mu}{\beta}(\gamma_m^p u_l^{sh} + \gamma_l^p u_m^{sh}) \tag{2.35c}$$

Because the surface displacements and tractions are specified, using a plane wave approximation,

the kernels, **G** and **Σ** can be approximated by their far-field values with no additional loss of precision. The far-field approximation, which is valid when the separation between the receiver and the surface, S, is many times larger than the seismic wavelength (i.e., $Rk >> 1$), amounts to neglecting the R^{-2} and R^{-3} terms in equations (2.9) and (2.10). Applying the far-field approximation and then separating the resulting equations into parts propagating at the P wave and S wave velocities results in

$$G_{mn}^{\alpha} \approx \frac{1}{4\pi\rho\omega^2 R}[\gamma_m \gamma_n k_\alpha{}^2 e^{ik_\alpha R}] \tag{2.36a}$$

$$G_{mn}^{\beta} \approx \frac{1}{4\pi\rho\omega^2 R}[(\delta_{mn} - \gamma_m \gamma_n) k_\beta{}^2 e^{ik_\beta R}] \tag{2.36b}$$

$$\Sigma_{lmn}^{\alpha} \approx \frac{i\omega}{4\pi R\,\alpha}[(1-2\nu^2)\delta_{lm}\gamma_n + 2\nu^2\gamma_l\gamma_m\gamma_n]\, e^{ik_\alpha R} \tag{2.37a}$$

$$\Sigma_{lmn}^{\beta} \approx \frac{i\omega}{4\pi R\,\beta}[\delta_{mn}\gamma_l + \delta_{ln}\gamma_m - 2\gamma_l\gamma_m\gamma_n]\, e^{ik_\beta R} \tag{2.37b}$$

where $\nu = \beta/\alpha$.

For the 2.5D geometry the components of **u**, **τ**, **G** , and **Σ** involving γ_2^{sh} and γ_3^{sh} are zero. If, in addition, the source does not excite SH waves, the components involving γ_1^{sh} are also zero.

The displacement at the receiver is obtained from either the 3D or 2.5D equations (2.29a) and (2.29b) by substituting the given expressions for the displacement and stress obtained from geometric ray theory and the far-field expressions for the Green's displacement dyadic and Green's stress tensor and evaluating the integral numerically (discussed in Section 2.2.5). This procedure can be viewed as a four step process: (1) ray trace from source to surface, (2) calculate the surface tractions assuming a plane wave, (3) propagate the wavefield across the surface using plane wave transmission and reflection coefficients, and (4) propagate the wavefield from surface to receiver using the free-space Green's function.

In this section, it was assumed that the medium is homogeneous. The Kirchhoff method can be used to model waves in an inhomogeneous medium as well if expressions for the surface displacements and the Green's function are available. Geometric ray theory expressions for inhomogeneous media (Aki and Richards, 1980) can be used to approximate the surface displacements. An approximate Green's function for a general inhomogeneous medium can be obtained either from geometric ray

theory (Frazer and Sen, 1985; Frazer, 1987; Sen and Frazer, 1985, 1987) or through an asymptotic analysis of the free-space Green's function (Cohen, 1988; Sumner, 1988).

2.2.4 Plane Wave Transmission and Reflection Coefficients for a Fracture

In the previous section, all the necessary terms in the Kirchhoff integral were specified with the exception of the plane wave transmission and reflection coefficients. Transmission and reflection coefficients for a plane wave incident upon an interface between two elastic media or a free-surface are well known (Aki and Richards, 1980). In this section, transmission and reflection coefficients for a plane wave incident upon a fracture are given.

A fracture is modeled as a planar, non-welded contact that is infinitesimally thin but that is many times larger than the seismic wavelength in its other two dimensions. In this model, traction is continuous across the fracture but displacement is discontinous. The magnitude of the displacement discontinuity is controlled by the stiffness of the fracture.

The displacement discontinuity model of a non-welded contact between two elastic media was introduced in the geophysics literature by Shoenberg (1980). Equivalent models have been used in non-destructive evaluation studies of flaws and cracks in engineering materials (Buck et. al., 1987). Pyrak (1988) investigated the effects of stress, pore fluids, and temperature on the transmission of ultrasonic waves across single natural fractures in crystalline rock specimens and obtained experimental results that showed good agreement with the this model.

In the displacement discontinuity model for wave propagation across a non-welded contact, the boundary conditions are: (1) continuity of stress, and (2) discontinuity in displacement proportional to the stress divided by the stiffness of the contact:

$$\tau_{lm}{}^{1} = \tau_{lm}{}^{2} \tag{2.38a}$$

$$u_l{}^{1} - u_l{}^{2} = \frac{\tau_{lm}}{K_l} \tag{2.38b}$$

where $\mathbf{u}$ is the displacement, $\boldsymbol{\tau}$ is the stress tensor, $\mathbf{K}$ is the specific stiffness of the non-welded contact, and the superscripts 1 and 2 refer to the material above and below the contact, respectively.

For a fluid-filled fracture, the effect of the specific viscosity of the fluid must also be included. The boundary conditions for a fluid-filled fracture are (Pyrak, 1988)

$$\tau_{lm}{}^{1} = \tau_{lm}{}^{2} \tag{2.39a}$$

$$K_l(u_l{}^{1} - u_l{}^{2}) + \eta\left[\frac{\partial u_l{}^{1}}{\partial t} - \frac{\partial u_l{}^{2}}{\partial t}\right] = \tau_{lm} \tag{2.39b}$$

where η is the specific viscosity and $\mathbf{K}$ now includes the stiffness due to the incompressibility of the fluid, in addition to the stiffness of the fracture solid contact areas.

These boundary conditions represent constitutive relations between local stress and displacement across the crack. For the two limiting cases $\mathbf{K} \rightarrow 0$ and $\mathbf{K} \rightarrow \infty$, these relations describe a free-surface and a welded contact, respectively. For intermediate values of $\mathbf{K}$, they describe a non-welded contact.

Plane wave reflection and transmission coefficients are calculated by substituting the expression for the plane wave displacement into the isotropic stress tensor and then applying the boundary conditions given above. The resulting systems of linear equations for an incident P wave, an incident SV wave, and an incident SH wave are

$$\mathbf{A}\,\mathbf{x}^{p} = \mathbf{b}^{p} \qquad \mathbf{A}\,\mathbf{x}^{sv} = \mathbf{b}^{sv} \qquad \mathbf{A}\,\mathbf{x}^{sh} = \mathbf{b}^{sh} \tag{2.40}$$

For a plane P or SV wave incident upon a dry fracture, the 4x4 coefficient matrix, $\mathbf{A}$, and the two column vectors, $\mathbf{x}$ and $\mathbf{b}$, are (Pyrak, 1988)

$$\mathbf{A} = \begin{bmatrix} -K_z\cos\theta_1 & K_z\sin\phi_1 & -K_z\cos\theta_2 + i\,\omega Z_{p_2}\cos 2\phi_2 & K_z\sin\phi_2 - i\,\omega Z_{s_2}\sin 2\phi_2 \\ -K_x\sin\theta_1 & -K_y\cos\phi_1 & K_x\sin\theta_2 - i\,\omega(Z_{s_2}{}^{2}/Z_{p_2})\sin 2\theta_2 & K_x\cos\phi_2 - i\,\omega Z_{s_2}\cos 2\phi_2 \\ -Z_{p_1}\cos 2\phi_1 & Z_{s_1}\sin 2\phi_1 & Z_{p_2}\cos 2\phi_2 & -Z_{s_2}\sin 2\phi_2 \\ (Z_{s_1}{}^{2}/Z_{p_1})\sin 2\theta_1 & Z_{s_1}\cos 2\phi_1 & (Z_{s_2}{}^{2}/Z_{p_2})\sin 2\theta_2 & Z_{s_2}\cos 2\phi_2 \end{bmatrix} \tag{2.41}$$

$$\mathbf{x}^{p} = \begin{bmatrix} R^{pp} \\ R^{ps} \\ T^{pp} \\ T^{ps} \end{bmatrix}, \qquad \mathbf{x}^{sv} = \begin{bmatrix} R^{sp} \\ R^{ss} \\ T^{ss} \\ T^{sp} \end{bmatrix} \tag{2.42}$$

$$\mathbf{b}^{p} = \begin{bmatrix} A_{11} \\ -A_{21} \\ -A_{31} \\ A_{41} \end{bmatrix} \quad , \quad \mathbf{b}^{sv} = \begin{bmatrix} A_{12} \\ -A_{22} \\ -A_{32} \\ A_{42} \end{bmatrix} \tag{2.43}$$

For a plane SH wave incident upon a dry fracture, **A** is given by the following 2x2 matrix

$$\mathbf{A} = \begin{bmatrix} -K_x & K_x - i\omega Z_{s_2}\cos\phi_2 \\ Z_{s_1}\cos\phi_1 & Z_{s_2}\cos\phi_2 \end{bmatrix} \tag{2.44}$$

$$\mathbf{x}^{sh} = \begin{bmatrix} R^{sh} \\ T^{sh} \end{bmatrix} \quad , \quad \mathbf{b}^{sh} = \begin{bmatrix} -A_{11} \\ A_{21} \end{bmatrix} \tag{2.45}$$

where $Z_{p_i}=\rho_i\alpha_i$ and $Z_{s_i}=\rho_i\beta_i$ are P wave and S wave acoustic impedances; θ_i and ϕ_i are the angles between the surface normal and the P and SV wavefront normals, respectively; and the subscript i=1,2 refers to the medium above and below the surface. Similar expressions for **A** have been derived for fluid-filled fractures (Pyrak, 1980). In this study, only dry fractures are considered.

Figure 2.6 shows the displacement discontinuity theory transmission coefficients as a function of frequency for a P wave at normal incidence. The various curves are for different stiffness values. Because of the frequency dependence of the reflection and transmission coefficients, a plane wave incident upon a non-welded contact will experience a reduction in amplitude and a loss of its high frequency content.

The frequency dependence of the transmitted and reflected waves from a displacement discontinuity theory and a thin layer are not identical. Peterson (personal communication) compared the transmission coefficients for a plane P wave at normal incidence to a fracture with those for a thin layer (Rayleigh, 1945). He found that he could match the frequency dependence of the two models by adjusting the elastic parameters of the thin layer. However, matching the transmission coefficients often required unrealistic values for the elastic parameters of the thin layer.

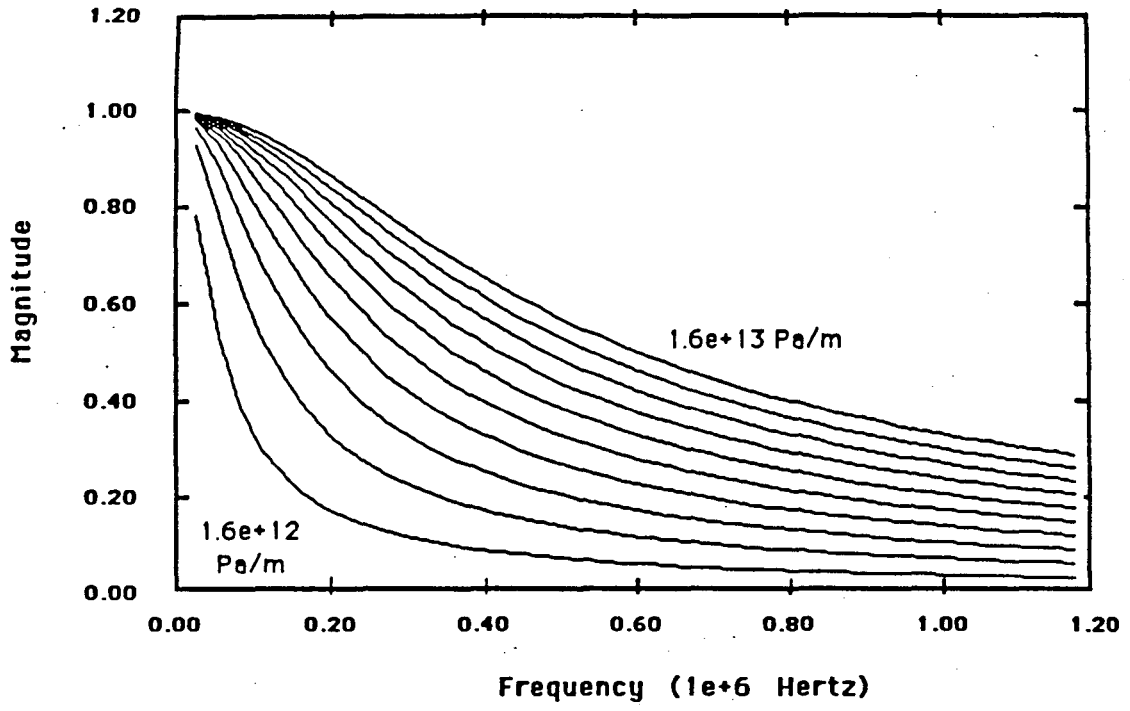

Figure 2.6 P wave transmission coefficients (normal incidence) as a function of frequency. The different curves are for stiffnesses ranging from 1.6e+13 Pa/m to 1.6e+12 Pa/m (from Pyrak, 1988).

2.2.5 Numerical Evaluation of the Kirchhoff Integral

Numerical quadrature of the 3D and 2.5D Kirchhoff integrals (equation (2.29a) and (2.29b), respectively) using the trapezoidal rule requires a large number of integration steps when ω is large. Scott (1985) found that surfaces with moderately irregular topography required a step size proportional to $\frac{c}{f}$, where f is the highest frequency transmitted and $c=\beta$.

A more efficient quadrature method has been presented by Sen and Frazer (1987). Their approach is based on the generalized Filon method (GFM) quadrature formula for oscillatory integrals. This approach is claimed to reduce the integration step size to $\frac{c}{\sqrt{f}}$. Most of the surfaces in the examples presented in the following chapter are smooth and not very large so that either the trapezoidal or Simpson's rule can be used without significantly sacrificing computation speed or accuracy.

The 2.5D and 3D Kirchhoff integrals given by equations (2.29a) and (2.29b) are for a monochromatic waves in an elastic medium. The time domain displacement resulting from a bandlimited source is obtained by solving equation (2.29a) and (2.29b) numerically for a range of frequencies and then performing an inverse Fourier transform of $\mathbf{u}(\mathbf{r},\omega)$. Sumner (1988) and Sen and Frazer (1987) demonstrated that it is possible to perform an analytical inverse Fourier transform of equations (2.29a) and (2.29b) when the material properties are frequency independent and a particular source function is assumed. From a computational standpoint it is advantageous to use the time domain Kirchhoff integral because synthetic seismograms can be computed for arbitrary time intervals. In this study, the transmission and reflection coefficients for a fracture are frequency dependent so an analytical inverse Fourier transform of the Kirchhoff integral is not attempted. The inverse Fourier transform is calculated numerically using an FFT (fast Fourier transform) routine.

2.3 Discussion

In this chapter, the Kirchhoff approximation was applied to the integral representation theorem for elastic waves. It was shown that this approximation uses geometrical ray theory to approximate the unknown boundary displacements and tractions and plane wave reflection and transmission coefficients

to propagate waves across the boundary. By approximating the boundary displacements and tractions using geometrical ray theory, we are effectively neglecting the contribution of multiply scattered waves, interface waves, and head waves.

The Kirchhoff method is an attractive numerical modeling method for three dimensional, elastic problems. For most problems, it is many times faster than non-asymptotic methods such as finite difference, finite element, and boundary integral equation methods. Furthermore, because it is an asymptotic method, each phase can be computed separately providing physical insight to the results. Ray theory offers similar benefits but unlike the Kirchhoff method, it does not model diffractions and it fails when there is a caustic at the receiver.

However, because of the Kirchhoff method is an asymptotic method it will produce inaccurate results if certain conditions are violated. Numerous studies have shown that the Kirchhoff method fails to give accurate results for large offsets between source and receiver and where there are rapid variations in the surface topography (Thoros, 1988; Jebsen and Medwin, 1982; Wirgin, 1989; Paul and Campillo, 1988). The results for a receiver in the near-field of the source (less than several wavelengths) will also be erroneous since the far-field approximation was used to simplify the Green's displacement and stress tensors and because the high frequency approximation is implicit in the Kirchhoff method. Recently, several restrictions on the Kirchhoff method have been partially lifted. Frazer and Sen (1985), Sen and Frazer (1985, 1987), and Frazer (1987) have presented approaches for dealing with head waves and the case when there is a caustic on the boundary surface.

The Kirchhoff method can be applied to model wave propagation across fractures if the properties of the fracture can be represented by plane wave transmission and reflection coefficients. The displacement discontinuity model of a fracture presented in this chapter is formally defined for fractures of infinite width and infinitesimal thickness (compared to a seismic wavelength). In this study, we are interested in the diffractions from the edges of fractures and, consequently, fractures are allowed to have a finite width. The Kirchhoff method will give correct travel times for the diffracted waves when the Kirchhoff approximation holds. Dalton and Yedlin (1988) have compared an exact and Kirchhoff method solution for acoustic diffraction from a half-plane and found that discrepancies exist in the

amplitude of the diffracted waves that becomes more severe with increasing source-receiver separation. In Section 3.4, an approach for treating diffracted waves from the fracture edge will be addressed.

At this point it is worth comparing the approach of this study with the approach typically used in solving elastic wave scattering in an infinite medium containing a single crack (Achenbach et. al., 1982; Mal, 1982). In crack problems, two surfaces of the crack are considered

$$\mathbf{u}(\mathbf{r},\omega) = \int_{S^+ + S^-} [\tau(\mathbf{r}',\omega)\mathbf{G}(\mathbf{r}|\mathbf{r}',\omega) - \mathbf{u}(\mathbf{r}',\omega)\boldsymbol{\Sigma}(\mathbf{r}|\mathbf{r}',\omega)]\cdot\hat{n}\ dS \tag{2.46}$$

where S^+ and S^- denote the upper and lower surfaces of the crack. Noting that the crack faces are traction free reduces equation (2.40) to

$$\mathbf{u}(\mathbf{r},\omega) = -\int_S [\mathbf{u}(\mathbf{r}',\omega)]\boldsymbol{\Sigma}(\mathbf{r}|\mathbf{r}',\omega)\cdot\hat{n}\ dS \tag{2.47}$$

where $[u] = u^+ - u^-$ is the crack opening displacement (COD).

It may appear tempting to substitute equation (2.38b), which has the form of a quasi-static COD, directly into equation (2.47). If this is done, it is immediately apparent that $[u]\rightarrow 0$ as $\mathbf{K}\rightarrow\infty$ and the transmitted wavefield approaches zero as the contact becomes perfectly welded. This seeming contradiction occurs because implicit in the derivation of equation (2.47) is the assumption that the crack faces never come into contact.

In the displacement discontinuity model, asperities on the opposite faces of the crack are allowed to come into contact when the stiffness of the crack is large. Equation (2.47) along with equation (2.38b) can be used to compute the reflected wavefield without any modification. However, to compute the transmitted wavefield requires a minor modification of equation (2.47) (see Buck et. al., 1987).

CHAPTER 3

ELASTIC KIRCHHOFF SYNTHETICS FOR FRACTURE ROCK

3.1 Introduction

Geometric ray theory and propagator matrix methods have been used recently to generate synthetic seismograms for elastic wave propagation across fractures described by the displacement discontinuity theory (Majer et. al., 1986; Shoenberg, 1980, 1983). Each method has certain advantages and shortcomings. Ray theory is capable of generating synthetics for multiple fractures with arbitrary orientation. Unfortunately, it gives a high frequency solution that it is restricted to planar fractures with uniform properties (e.g., constant stiffness) and that does not include diffractions from fracture edges. Ray theory is capable of modeling multiples and head waves but this will significantly increase computation time and in the case of multiples, it is restricted to fracture spacings that are large compared to the seismic wavelength. The propagator matrix method gives an exact solution that includes multiples without restriction on the spacing of the fractures. However, it is limited to fractures that are parallel and of infinite extent.

The elastic Kirchhoff method can be viewed as an extension of ray theory to handle diffractions, variations in surface properties of the fracture, and the particular situation where the receiver is located on a caustic. The tradeoff associated with selecting the Kirchhoff method over ray theory is an increase in computation time, since the equivalent of two ray traces per surface element are required.

This chapter first examines the accuracy of the Kirchhoff method as formulated with the plane wave transmission and reflection coefficients obtained from the displacement discontinuity model of a fracture. Several limitations of the method are discussed. Finally, elastic Kirchhoff results are presented for single and multiple fracture models.

3.2 Validation

Several recent studies have presented elastic Kirchhoff results for seismic reflection from laterally varying, multi-layered, elastic media. Frazer and Sen (1985) obtained elastic Kirchhoff results for P-P reflection from an acoustic/elastic vertical fault model consisting of water overlaying a rigid step struc-

ture that closely matched experimental model tank data. While their study and subsequent study (Sen and Frazer, 1987) have shown the utility and accuracy of the method for acoustic and acoustic/elastic problems, they do not present an example of a fully elastic problem accompanied with its exact solution.

Because the elastic Kirchhoff method has been used much less frequently than its acoustic counterpart, it is worthwhile to examine its accuracy for several simple cases with known solutions. To check the accuracy of the elastic Kirchhoff method, two tests were performed. These tests were aimed at evaluating the performance of Kirchhoff method transmission and reflection results for the limiting cases of total transmission and total reflection.

3.2.1 Free-Space Test

The first test consisted of a comparison of the free-space Green's function with the elastic Kirchhoff numerical results for a surface with infinite stiffness. To perform this test, a point source and receiver were placed on opposite sides of a planar 2.5D surface 3 m wide in the y-direction and infinitely long in the x-direction. The normal and tangential stiffnesses were set at large values (1×10^{30} Pa/m) to simulate a welded contact with the material properties on either side of the contact identical (α=5600 m/s, β=4000 m/s, and ρ=2600 kg/m^3). The displacement discontinuity plane wave transmission coefficients calculated from equations (2.41)-(2.43) are shown in Figure 3.1. The surface was discretized into 100 line elements 0.1 m in length. The source wavelet used to produce the synthetics in this study (unless indicated otherwise) is a 6 kHz Ricker wavelet (Figure 3.2). The results from the 2.5D Kirchhoff algorithm given in Appendix A are compared with the far-field part of the free-space Green's function (equations (2.36a-b)) for three different orientations of the point source (Figure 3.3a-3.3c).

The 2.5D Kirchhoff results for all three source orientations show good agreement with the far-field, free-space Green's function. In the three examples, the x-components are zero because of the 2.5D geometry. The vertical point force (Figure 3.3a) generates only a P wave with particle motion purely in the z-direction. The horizontal point force (Figure 3.3b) generates only an SV wave with particle motion purely in the y-direction. These results are expected since source and receiver are either

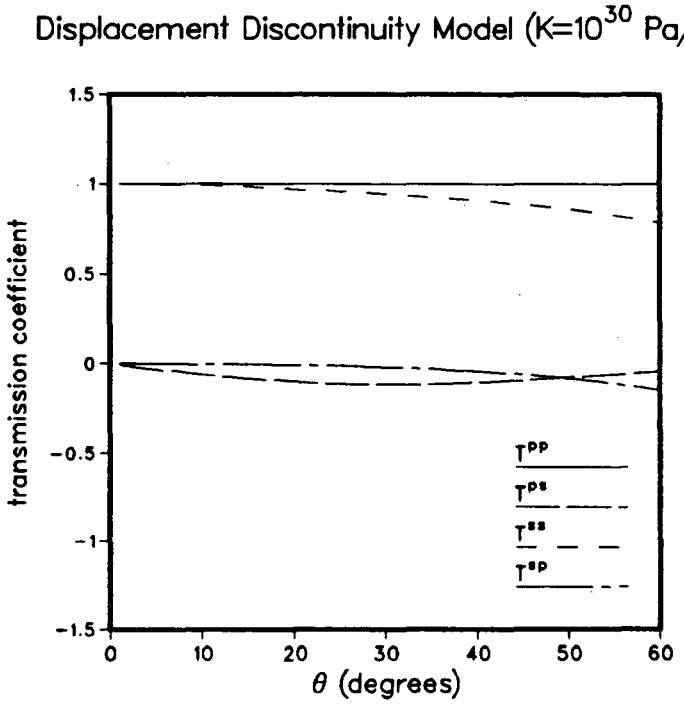

Figure 3.1 Plane wave transmission coefficients for incident P and SV waves and a stiffness of 1e+30 Pa/m.

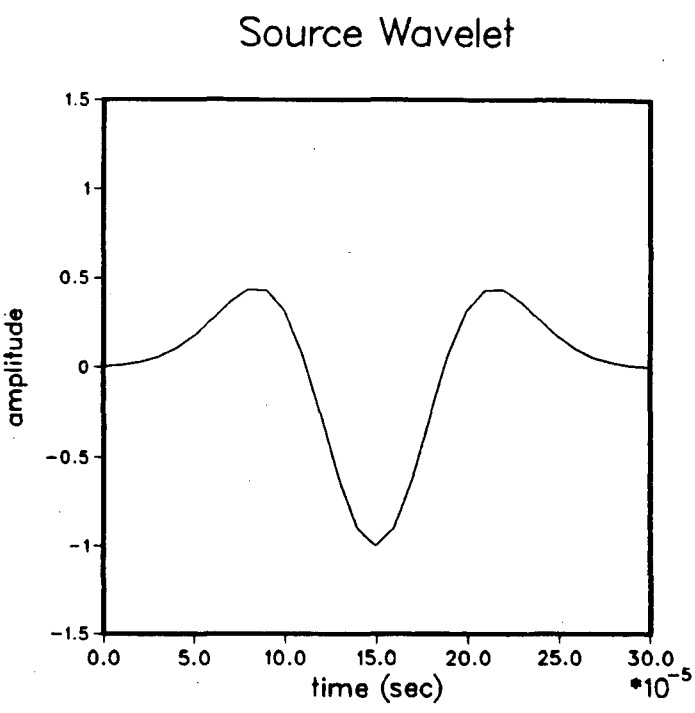

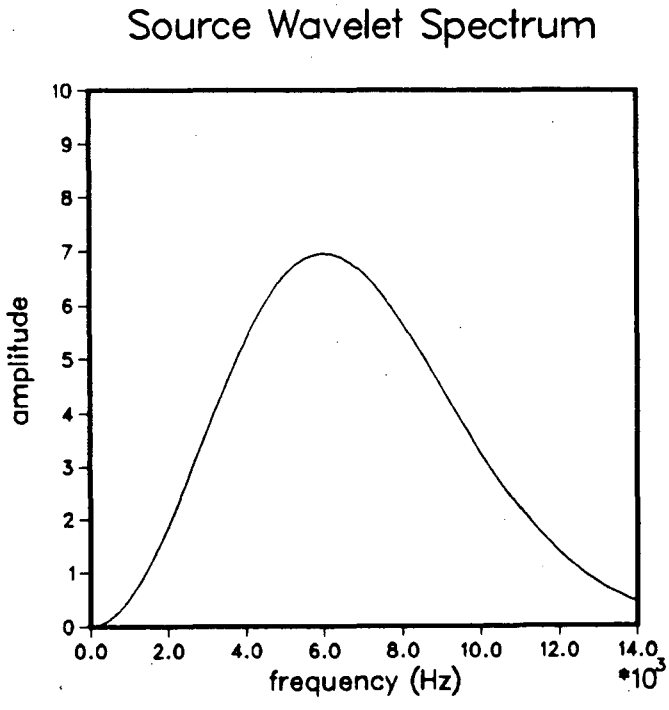

Figure 3.2 3-loop Ricker wavelet and its spectrum.

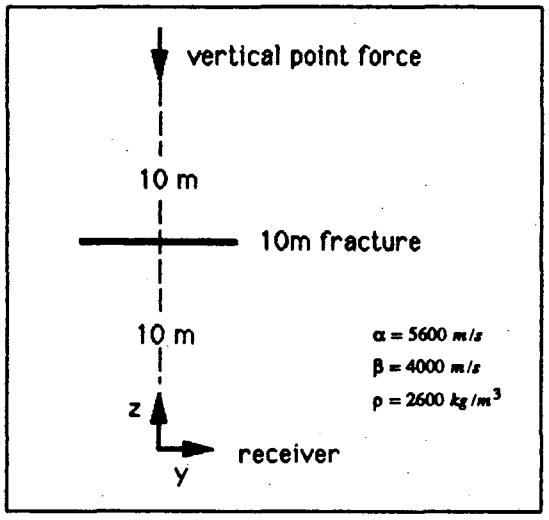

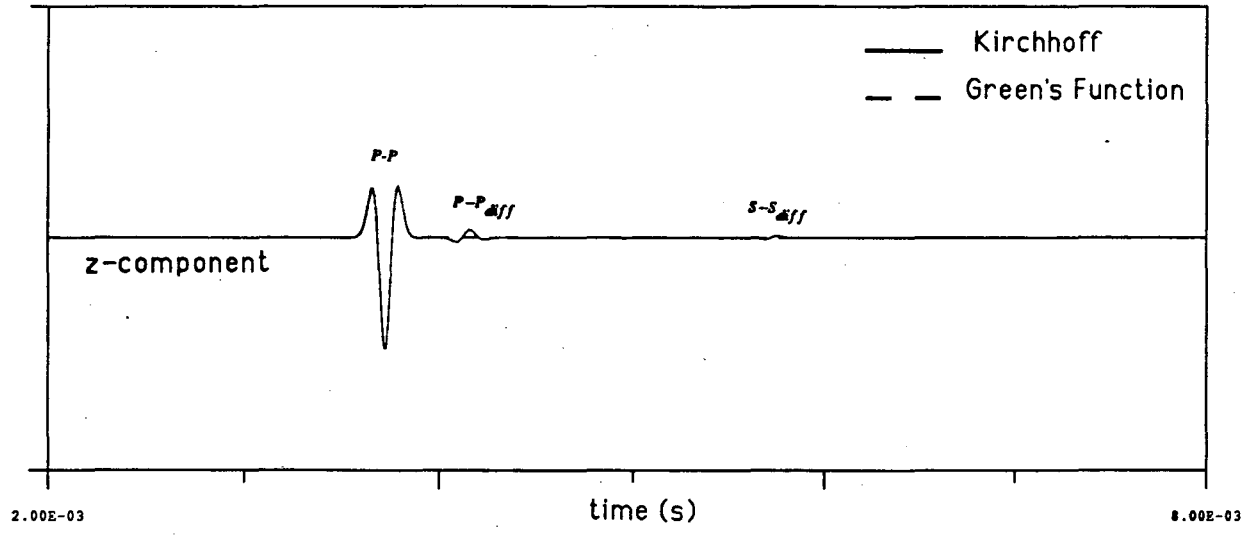

Figure 3.3a Comparision of the elastic Kirchhoff results and the far-field, free-space Green's function for a vertical point force.

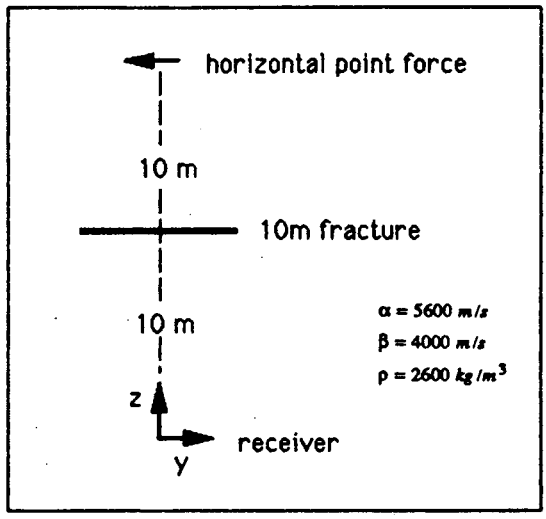

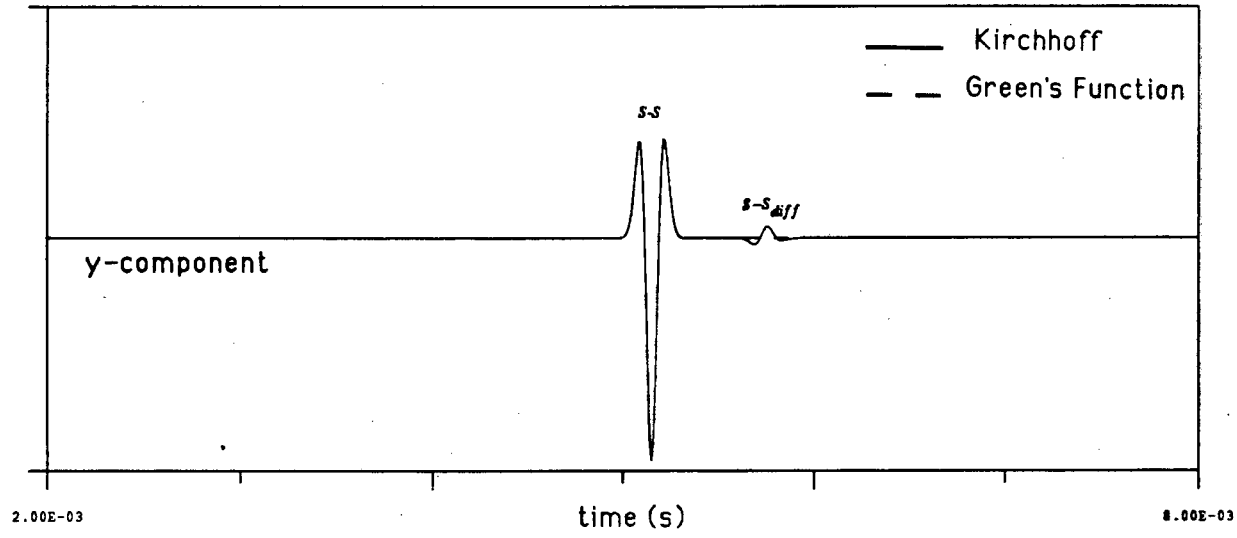

Figure 3.3b Comparision of the elastic Kirchhoff results and the far-field, free-space Green's function for a horizontal point force.

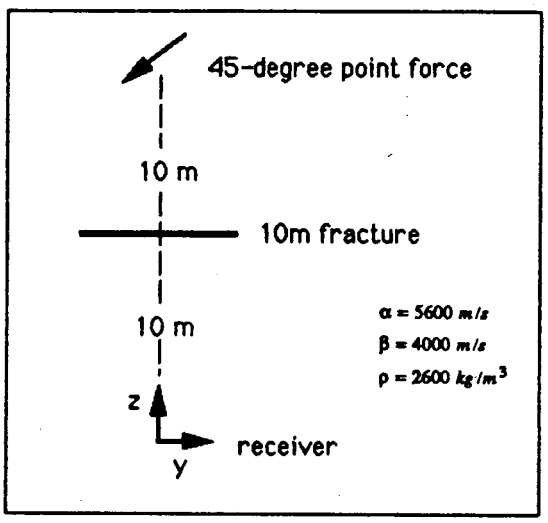

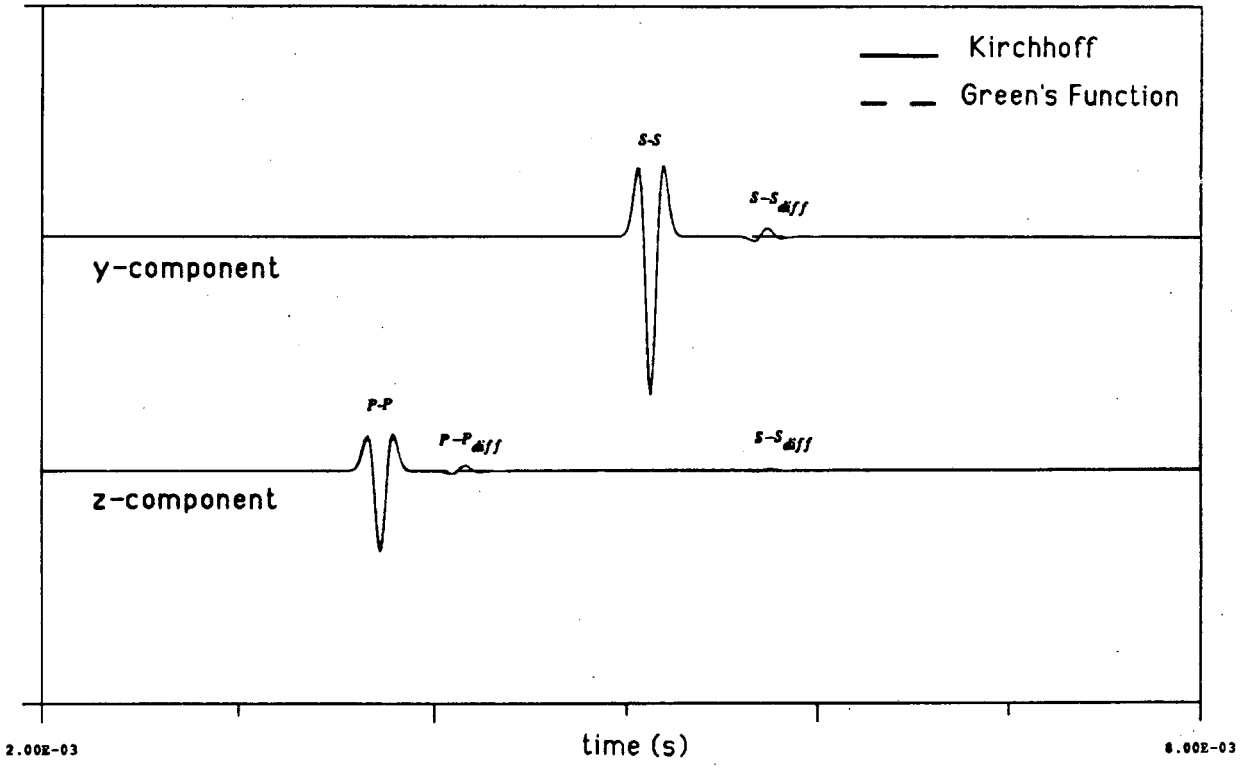

Figure 3.3c Comparision of the elastic Kirchhoff results and the far-field, free-space Green's function for a point force 45-degrees from vertical in the y-z plane.

perpendicular or parallel to the surface. The point force oriented at 45 degrees (Figure 3.3c) generates both P and SV waves that appear on the z- and y-components of displacement, respectively.

The only noticeable difference between the 2.5D Kirchhoff and the far-field free-space Green's function synthetics are the small amplitude waves in the Kirchhoff synthetics that arrive less than a millisecond after the P and SV waves. These arrivals are P-P, P-SV, SV-SV, and SV-P diffractions produced by the sharp changes in the transmission coefficients at the edges of the 2.5D surface (i.e., T^{pp} , T^{ps} , T^{ss} , and $T^{sp} \rightarrow 0$ at the fracture edges).

3.2.2 Free-Surface Test

The purpose of the second test was to check the Kirchhoff method elastic reflection results. The test consisted of a comparison of the Cagniard de-Hoop solution for an elastic half space (Johnson, 1976) with the 2.5D Kirchhoff numerical results for a surface with zero stiffness. The plane wave reflection coefficients for a free surface (Aki and Richards, 1980) and for a planar fracture surface with both normal and tangential stiffnesses set at 0.1 Pa/m are shown in Figure 3.4. The model consisted of a vertical point force and receiver that were both located 10 m below the free-surface and with an 8 m separation (Figure 3.5).

The time domain step response from the Cagniard de-Hoop code was convolved with the first derivative of the 3-loop Ricker wavelet (Figure 3.2). A comparison of the Kirchhoff and Cagniard de-Hoop results displayed in Figure 3.5 show fairly good agreement for the P-P, P-SV, and SV-P phases. The agreement begins to deteriorate for the SV-SV phase.

3.3 Limitations of the Elastic Kirchhoff Method

The elastic Kirchhoff transmission and reflection results of the preceding section give an optimistic measure of the accuracy of the method for simple models. However, there are several inherent problems with the method that will result in inaccurate solutions. As discussed in Section 2.3, errors in the amplitudes of the Kirchhoff solution result when the Kirchhoff approximation (Section 2.2.3) is violated. Thus, the Kirchhoff method should only be used to model high frequency waves in the far-field. The method should not be applied to problems involving rapid variations in the elastic properties or topography of the surface or large offsets between source and receiver.

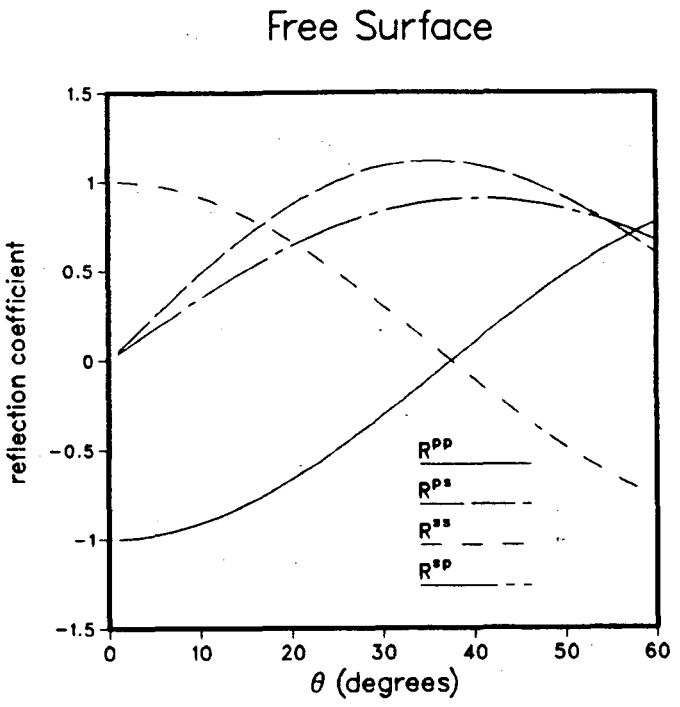

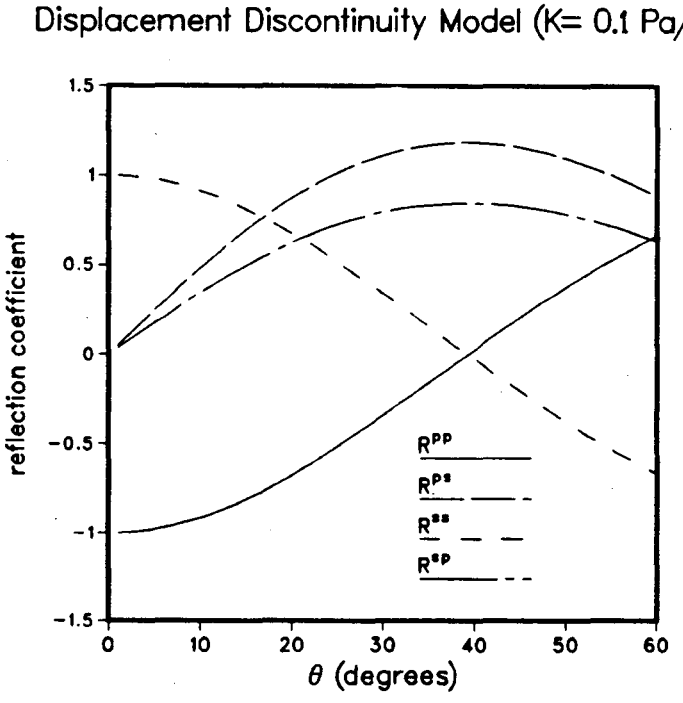

Figure 3.4 Comparision of the plane wave reflection coefficients for a free-surface and for the displacement discontinuity model with stiffness 1e-01 Pa/m.

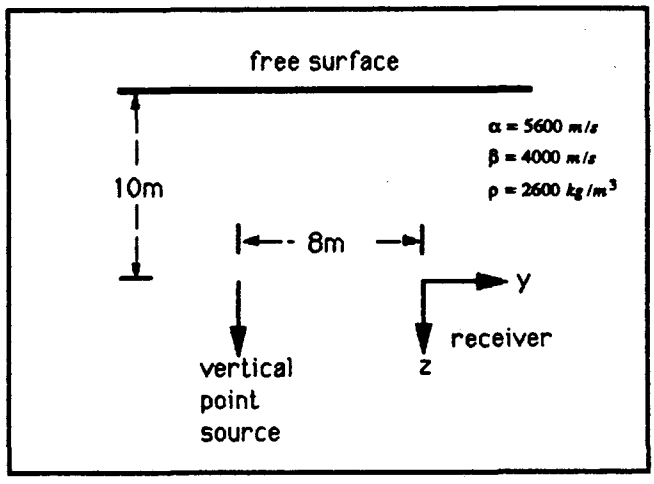

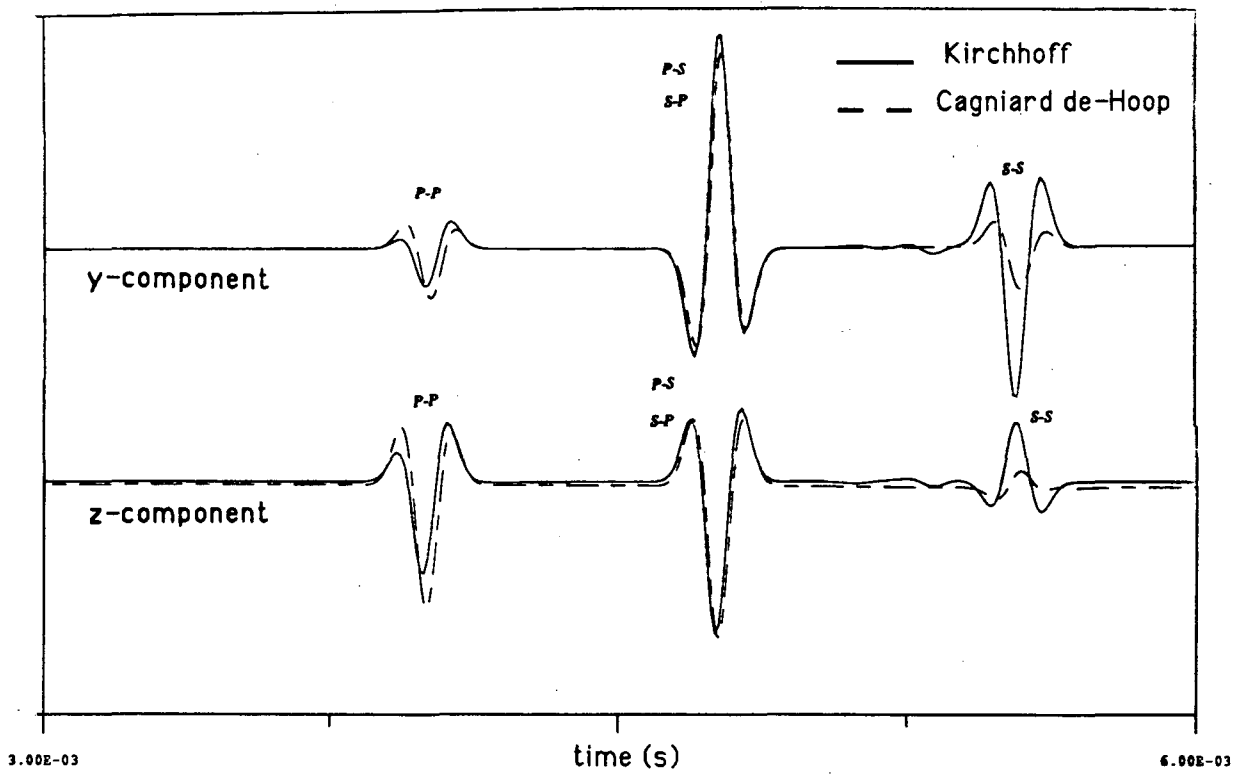

Figure 3.5 Comparision of the Kirchhoff and Cagniard reflection synthetics for a free-surface.

The problems mentioned above place limitations on the types of problem geometries the Kirchhoff method can be applied to. Errors that result from the violation of the Kirchhoff approximation tend to primarily affect the accuracy of the wave amplitudes.

The amplitudes of the Kirchhoff synthetics are only approximate and may be in error even in situations where the Kirchhoff approximation holds. This is largely due to the ad hoc method in which the transmission and reflection coefficients are computed. Computing the reflection and transmission coefficients requires that the angles of incidence, reflection, and transmission be specified. However, ray paths from source-to-surface and surface-to-receiver (Kirchhoff ray paths; e.g., Figure 2.1) are, in almost all instances, non-Snell's Law paths.

A problem that results from this ad hoc approach of computing the reflection and transmission coefficients results in inaccurate reflection results for small offsets between source and receiver. Figure 3.6 shows z-component of displacement computed using the 2.5D Kirchhoff code for coincident source and receiver. The surface is 8 m in the y-direction and infinite in the x-direction (i.e., 2.5D) and the source is a vertical point force. The y-component of displacement (not shown) is zero as predicted by geometrical ray theory. However, for the z-component, the first arrival should be the reflected P-P wave followed by smaller amplitude diffracted waves from the edges of the fracture. Instead, in addition to the P-P reflection and the edge diffracted waves, there are also large amplitude P-SV and SV-P reflected waves.

Two effects combine to produce these large amplitude waves: (1) the z-component of the SV wave particle motion becomes large as the angle of incidence increases (Figure 3.7), and (2) both the P-SV and SV-P reflection coefficients become large as the angle of incidence increases (Figure 3.4). Thus, for surfaces that are small in comparison to the distance from the source-receiver location to the surface, the P-SV and SV-P reflection coefficients are small and the amplitude of the anomalous converted waves will be small. However when the surface is comparable in size to the distance to the surface, there will be large converted waves for the reasons given above.

In Section 3.2.2, it was observed that the Kirchhoff method was capable of producing acceptable results when the source and receiver are offset. It is postulated that an offset source and receiver results

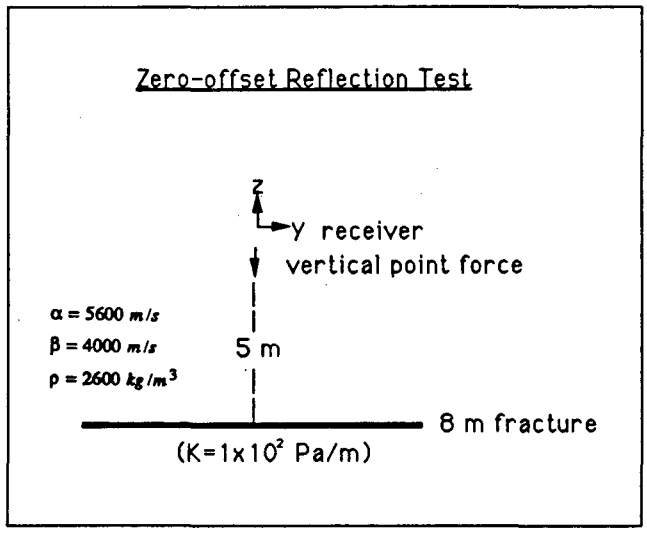

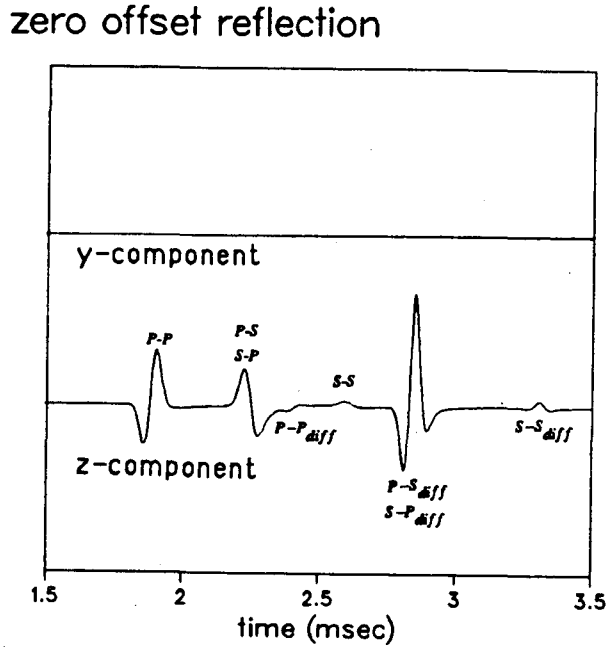

Figure 3.6 Kirchhoff synthetics for coincident source and receiver. Large amplitude anomalous converted waves appear after the P-P arrival.

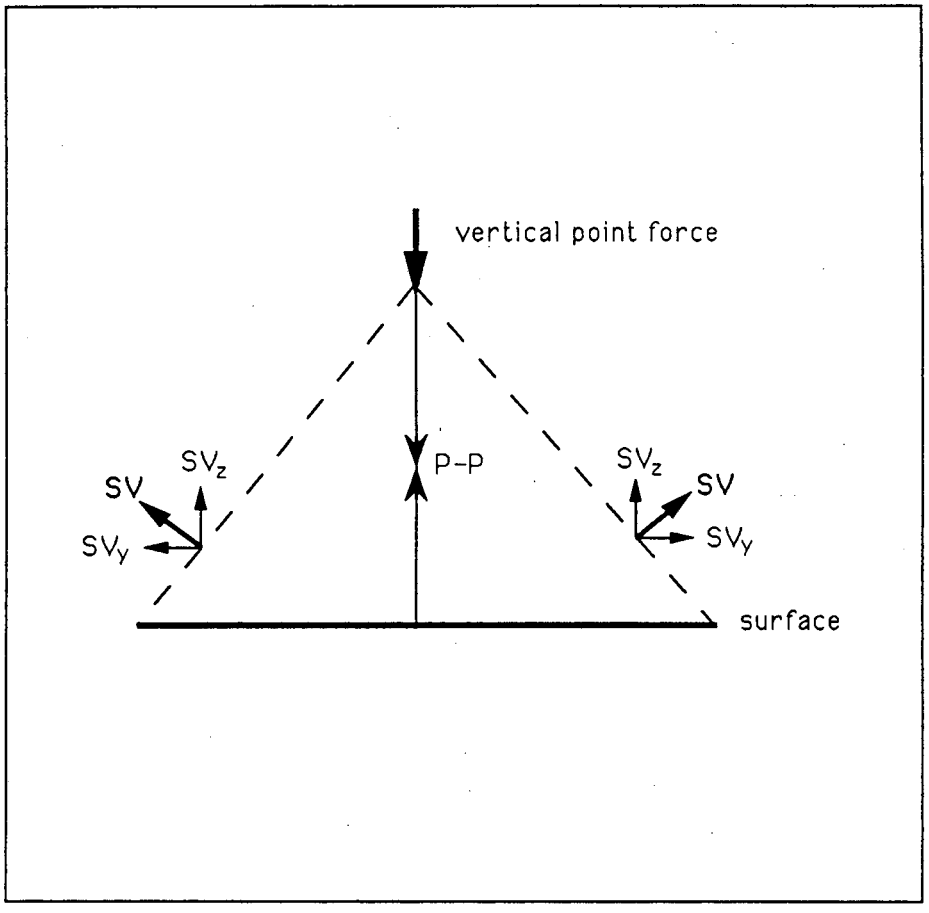

Figure 3.7 For a vertical point source and a flat surface, the z-component of the SV wave increases with increasing angle of incidence.

in greater cancellation of the anomalous converted waves except over portions of the surface associated with specular reflection.

The large amplitude P-SV and SV-P waves can be removed by tapering R^{PS} and R^{SP} such that these reflection coefficients are small at large angles of incidence. An equivalent approach that has perhaps some physical appeal is to vary the stiffness from a small value at the fracture center to a large value at the fracture edge.

It is interesting to note that the elastic Kirchhoff method for normal incidence transmission does not suffer from this problem because the transmission coefficients are usually small at large angles of incidences. Furthermore, because this failure at small source-receiver offsets stems from the behavior of the SV wave and the reflection coefficients of the converted waves, it should not occur in the acoustic Kirchhoff method.

3.4 Single Fracture Results

Kirchhoff transmission and reflection examples are presented in this section for fractures with stiffnesses of 1×10^{11} Pa/m (Figure 3.8) and 1×10^{29} Pa/m. The boundary conditions on the edges of a fracture should allow for complete transmission ($\mathbf{T} \rightarrow 1$) and zero reflection ($\mathbf{R} \rightarrow 0$) just off the fracture edge to properly describe welded rock. In the case of elastic wave reflection, the reflection coefficient is zero off the fracture edge and the edge boundary condition is satisfied. For elastic wave transmission, the transmission coefficient off of the fracture edge is zero and the boundary condition at the fracture edge is violated.

Incorporating the proper boundary condition at the fracture edge for elastic wave transmission requires incorporating a high stiffness surface that extends from the fracture edge. The extent of this surface should be large enough that diffractions from its outer edge have arrival times that are greater than the travel times of the waves of interest. Such a surface is shown in Figure 3.9 and the its synthetics in Figure 3.10. For a stiffness of 1×10^{29} Pa/m, there are no diffracted waves from the fracture edge, as expected. A fracture with a stiffness of 1×10^{11} Pa/m produces a P-P diffracted wave of visible amplitude on the first trace of the z-component of displacement. Converted and diffracted waves are present for both values of stiffness.

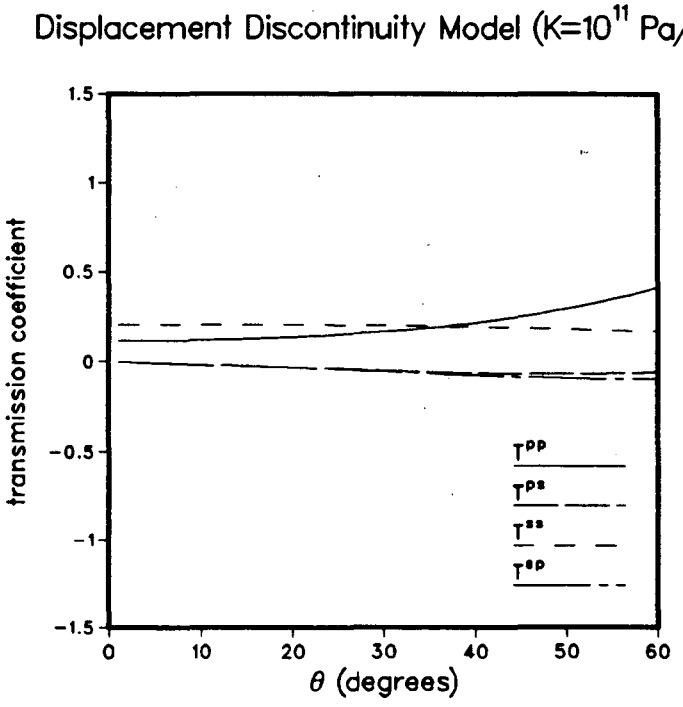

Figure 3.8 Plane wave transmission coefficients for a surface with stiffness 1e11 Pa/m.

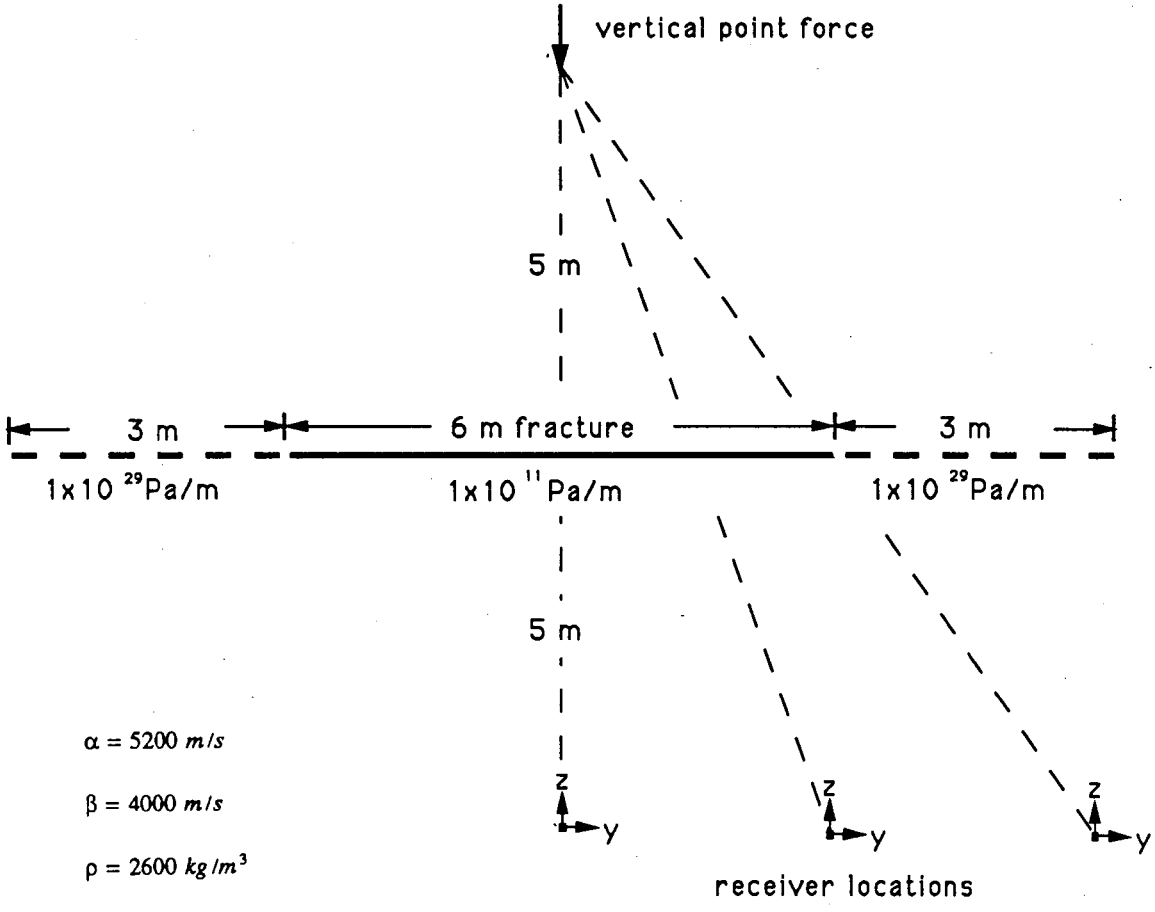

Figure 3.9 Constant stiffness fracture model used to generate the synthetics in Figure 3.10.

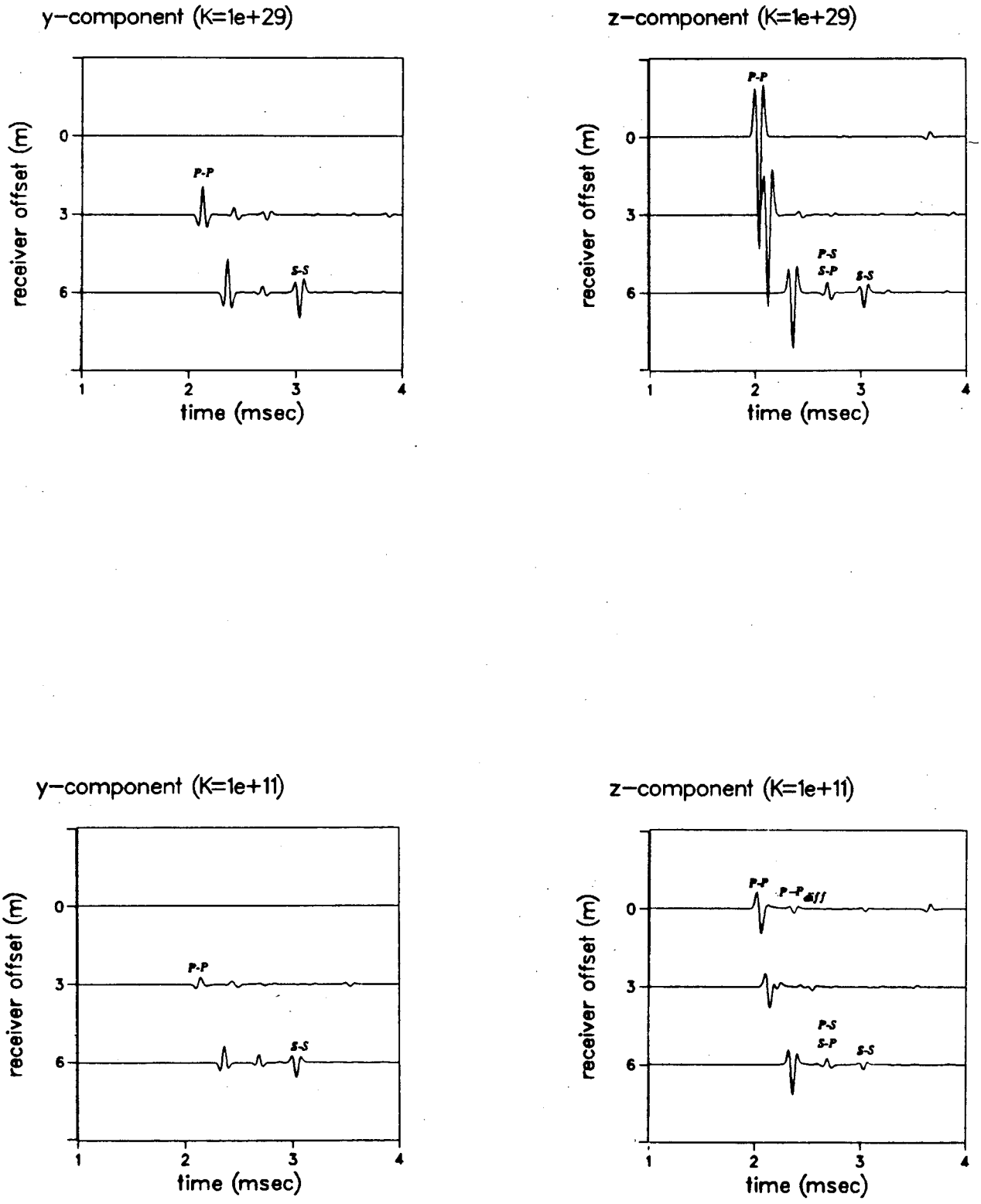

Figure 3.10 Kirchhoff transmission synthetics for the model shown in Figure 3.9.

To examine the frequency content of the transmitted waves, the spectra of the P-P wave for stiffnesses of 1×10^{11} Pa/m and 1×10^{29} Pa/m were computed for normal incidence transmission (i.e., zero offset). The spectra are displayed in Figure 3.11 (the source wavelet is a Ricker wavelet peaked at 10 kHz). It is clear from this figure that the fracture acts like a low pass filter for the fracture with the smaller stiffness.

The Kirchhoff reflection synthetics for the model displayed in Figure 3.12 are shown in Figure 3.13. These results should be viewed with some skepticism because of the problem which is encountered at small source-receiver offsets (Section 3.3). For a 6 m source-receiver offset, three major arrivals are apparent, in addition to the smaller amplitude diffracted waves.

The elastic Kirchhoff synthetics presented so far have been for flat surfaces with constant normal and tangential stiffnesses. For these simple surfaces, the Kirchhoff results will be identical to those produced by geometrical ray theory except that the Kirchhoff synthetics include diffractions from the fracture edges. In the following section, a fracture is again assumed to be planar, but the stiffness is allowed to vary spatially. For the Kirchhoff approximation to hold, the correlation length of the stiffness variations along the fracture surface must be large compared to the seismic wavelength. Also, for the same reason, the amplitude of the stiffness variations should be small.

The surfaces with a random stiffness distribution are generated using the approach described by Frankel and Clayton (1986). The surface is first discretized and assigned a random stiffness value taken from a uniform distribution. The FFT of this random stiffness surface is filtered with a Gaussian correlation function. The inverse FFT produces a random stiffness surface with a correlation length, a.

Random stiffness surfaces for two correlation lengths, a=0.5 m and a=0.2 m, and for a surface with a constant stiffness ($a=\infty$) are displayed in Figure 3.14. The random stiffness surfaces range in value from 1×10^{10} Pa/m to 1×10^{11} Pa/m. The constant stiffness surface has a stiffness of 5×10^{10} Pa/m. The Kirchhoff transmission synthetics are shown in Figure 3.15. The effects of the random surface are to attenuate the transmitted wave and remove a portion of its high frequency content. Identical effects were observed for transmission through a surface with random topography. In addition, the random stiffness surfaces excite scattered waves that appear on the y-component of displacement. These

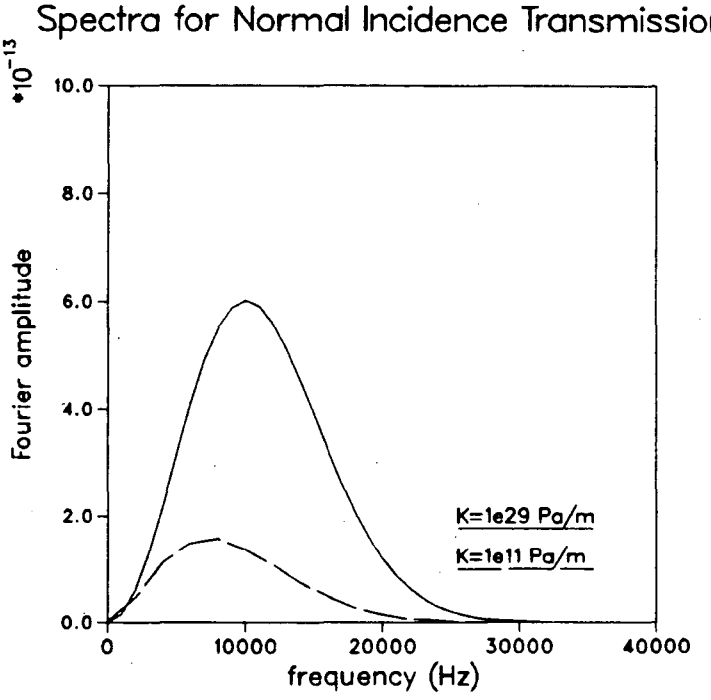

Figure 3.11 Comparison of the frequency content of a normally incident P-P transmitted wave of Figure 3.10 for fracture stiffnesses of K=1e29 Pa/m and K=1e11 Pa/m.

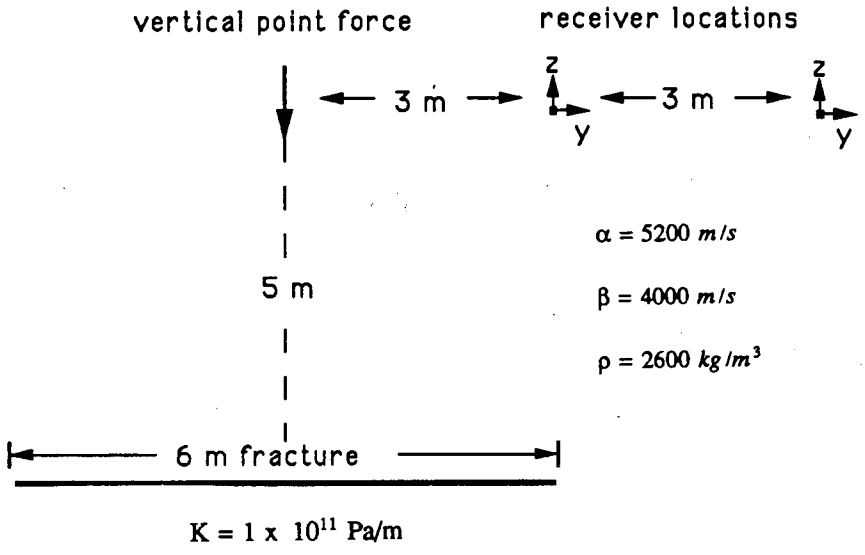

Figure 3.12 Constant stiffness fracture model used to generate the synthetics in Figure 3.13.

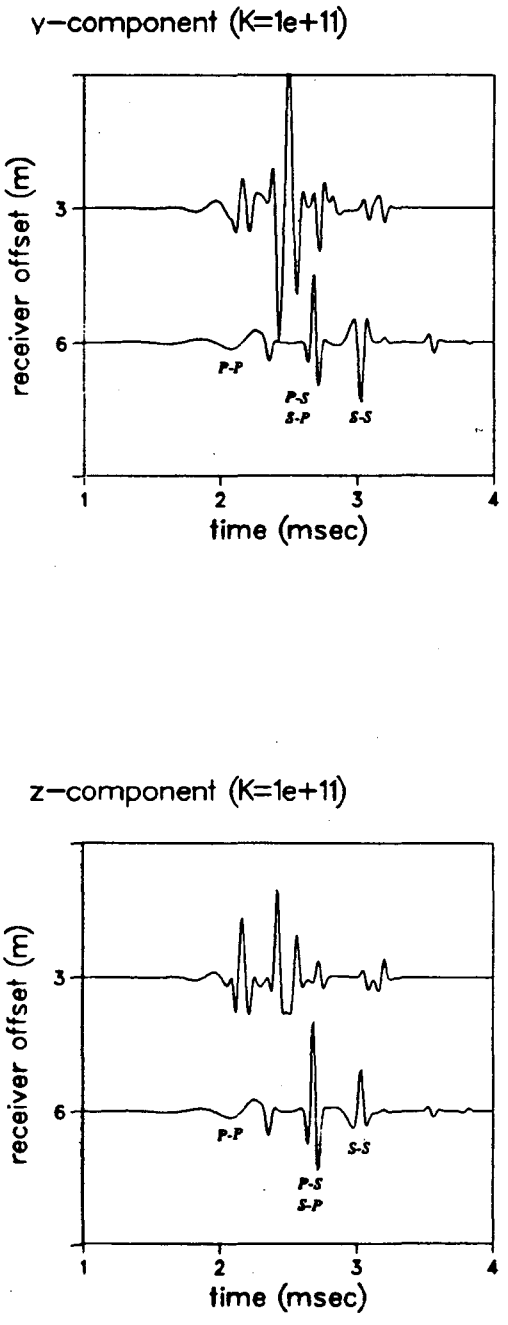

Figure 3.13 Kirchhoff reflection synthetics for the model shown in Figure 3.12.

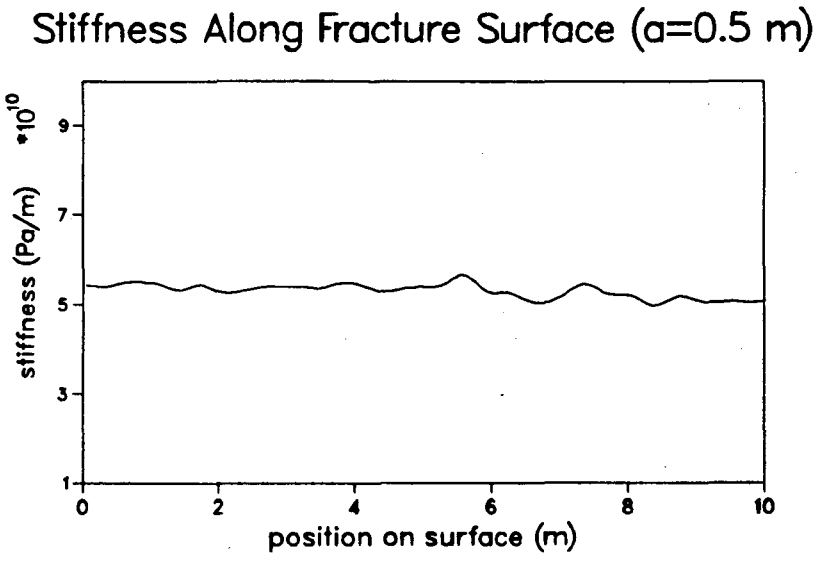

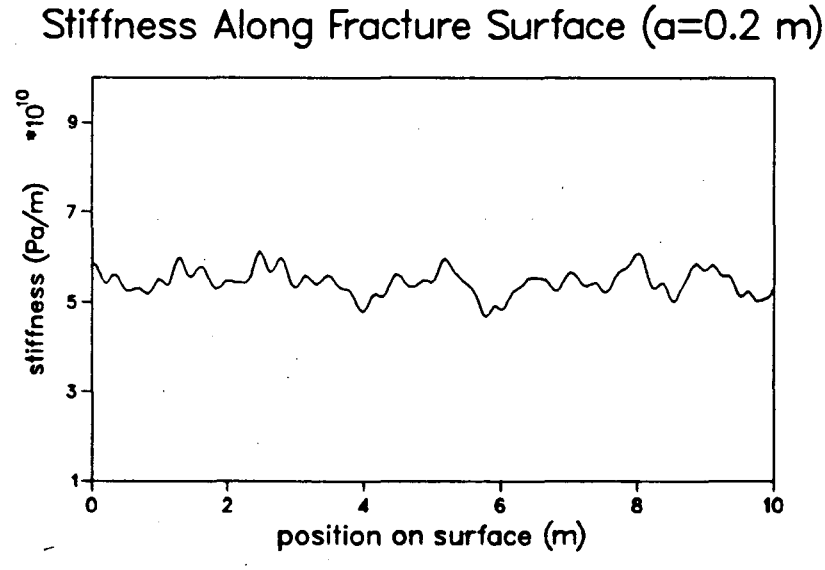

Figure 3.14 Random stiffness distributions along a 2.5D surface for Gaussian correlation lengths of a=0.5 m and a=0.2 m and stiffness values ranging from 1e10 Pa/m to 1e11 Pa/m.

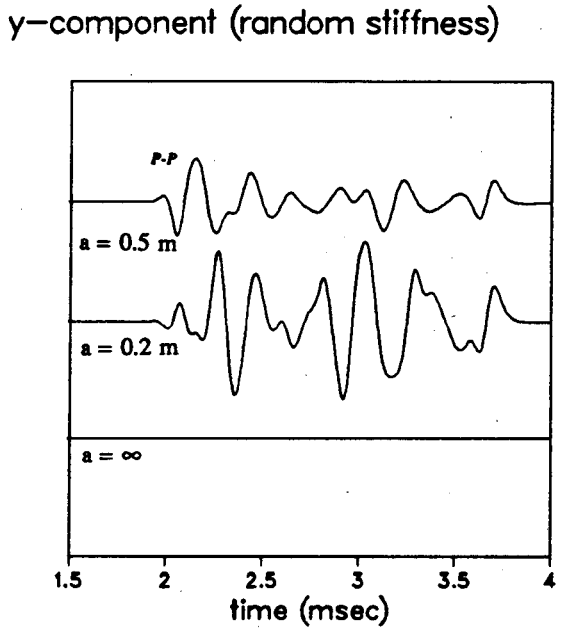

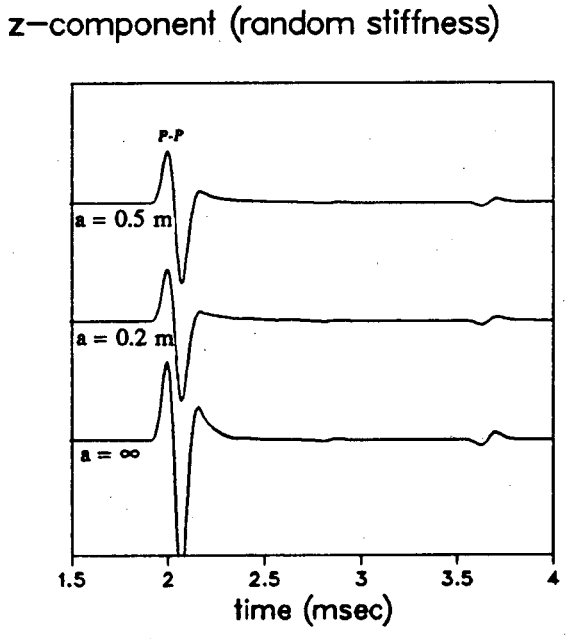

Figure 3.15 Kirchhoff transmission synthetics for the random stiffness models shown in Figure 3.14.

scattered waves are not present for a constant stiffness surface. The peak amplitude of the y-component is over 150 times smaller than z-component (y- and z-component traces are not scaled to each other) so that the scattered waves are not visible on the z-component since they are many times smaller than the P-P wave. The amplitude of the scattered waves increases as the correlation length decreases.

3.5 Multiple Fractures

The formalism presented in Chapter 2 for a single fracture can be extended to multiple fractures by performing additional integrations over each additional fracture surface. Multiple Kirchhoff integrals have been used recently by Frazer and Sen (1985, 1987) and Sumner (1988) to compute reflections from multi-layered elastic media. Frazer and Sen have labeled these integrals *multi-fold* path integrals because of their similarity to Feynman path integrals used in quantum mechanics.

For the problem of computing the elastic transmission through two fractures, the multiple Kirchhoff integral for the transmitted wave is

$$\mathbf{u}_n(\mathbf{r},\omega) = \int_{S_1}\int_{S_2} [\hat{n}_l{}^{(2)} t_{lm}{}^{(2)} G_{mn}{}^{(2\to1)} - v_m{}^{(2)}(\hat{n}_l{}^{(2)}\Sigma_{lmn}{}^{(2\to1)})]\, dS_2\, dS_1 \tag{3.1}$$

where $v_m{}^{(2)}$ and $t_{lm}{}^{(2)}$ are the displacements and stresses on the second fracture surface.

$$v_m{}^{(2)} = [\hat{n}_1{}^{(1)}\tau_{lm}{}^{(1)} G_{mn}{}^{(1\to2)} - u_m{}^{(1)}(\hat{n}_l{}^{(1)}\Sigma_{lmn}{}^{(1\to2)})] \tag{3.2}$$

$$t_{lm}{}^{(2)} = \tau(v_m{}^{(2)}) \tag{3.3}$$

This integral describes the transmitted wavefield shown in Figure 3.16.

The multiple Kirchhoff integral formalism is only valid if the separation between fractures is much larger than the seismic wavelength since the far-field approximation was invoked earlier. If either S_1 or S_2 is a smooth surface with uniform stiffness, the method of stationary phase can be applied to obtain an asymptotic solution of the corresponding integral. Diffractions from the edges of the surface will not be included in the stationary phase solution.

Multi-fold path integrals that include multiple reflections between fractures S_1 and S_2 can also be computed by performing additional integrals. However, modeling multiple reflections will result in a significant increase in computation time.

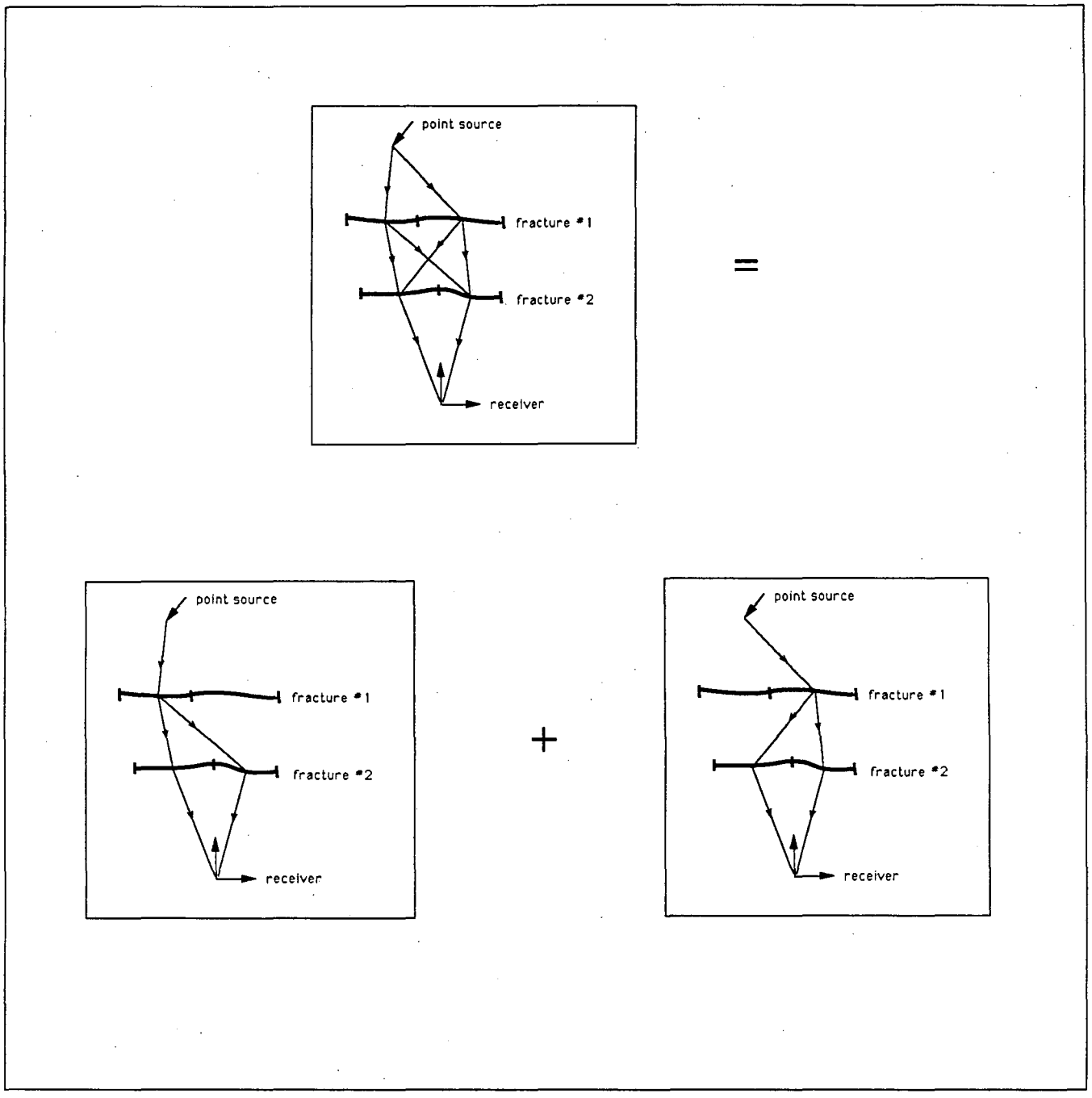

Figure 3.16 Physical representation of the multiple Kirchhoff integral.

Kirchhoff transmission synthetics for a two fractures, both with stiffnesses of 1×10^{11} Pa/m (Figure 3.17), are shown in Figure 3.18. The y- and z-components of displacement are displayed for three receiver locations. The vertical point source produces a P-P transmitted wave followed by smaller amplitude diffracted waves. For offset source and receiver, both transmitted and converted S waves appear on the y-component of displacement.

3.6 Discussion

The Kirchhoff method formalism for the 2.5D problem geometry presented in Chapter 2 was implemented in a FORTRAN code (see Appendix A). This code was used to examine the accuracy of the method and to generate synthetic seismograms for reflection and transmission from a fracture. The fracture was characterized by either a constant stiffness value or a random stiffness distribution.

An investigation of the accuracy of the Kirchhoff method revealed that the elastic Kirchhoff method fails to produce accurate reflection results for small offsets between the source and receiver. The inaccuracies appear in the form of large amplitude converted waves that should be small for small source-receiver offsets. This problem occurs because both the SV wave z-component of displacement and P-S and S-P plane wave reflection coefficients become large at large angles of incidence. The anomalous converted waves can be attenuated by tapering the P-S and S-P reflection coefficients when generating small source-receiver offset synthetics. The problem mentioned above did not seem to effect the results for larger source-receiver offsets.

The synthetics generated for transmission through a single fracture show that the amplitude and frequency content are directly related to the stiffness of the fracture. A fracture with a small stiffness tends to act like a low pass filter. This result is in direct agreement with experimental studies (Pyrak, 1980). The amplitude of the diffracted wave from the edge of the fracture is also larger for fractures with small stiffnesses. The amplitude of the diffracted waves from the fracture edge diminishes as the fracture becomes stiff (i.e., welded).

The results for transmission through a fracture with a random stiffness distribution reveals that scattered waves are generated at the fracture surface. The magnitude of the scattered waves increases as the correlation length decreases. The transmitted P-P wave shows that the effect of a random

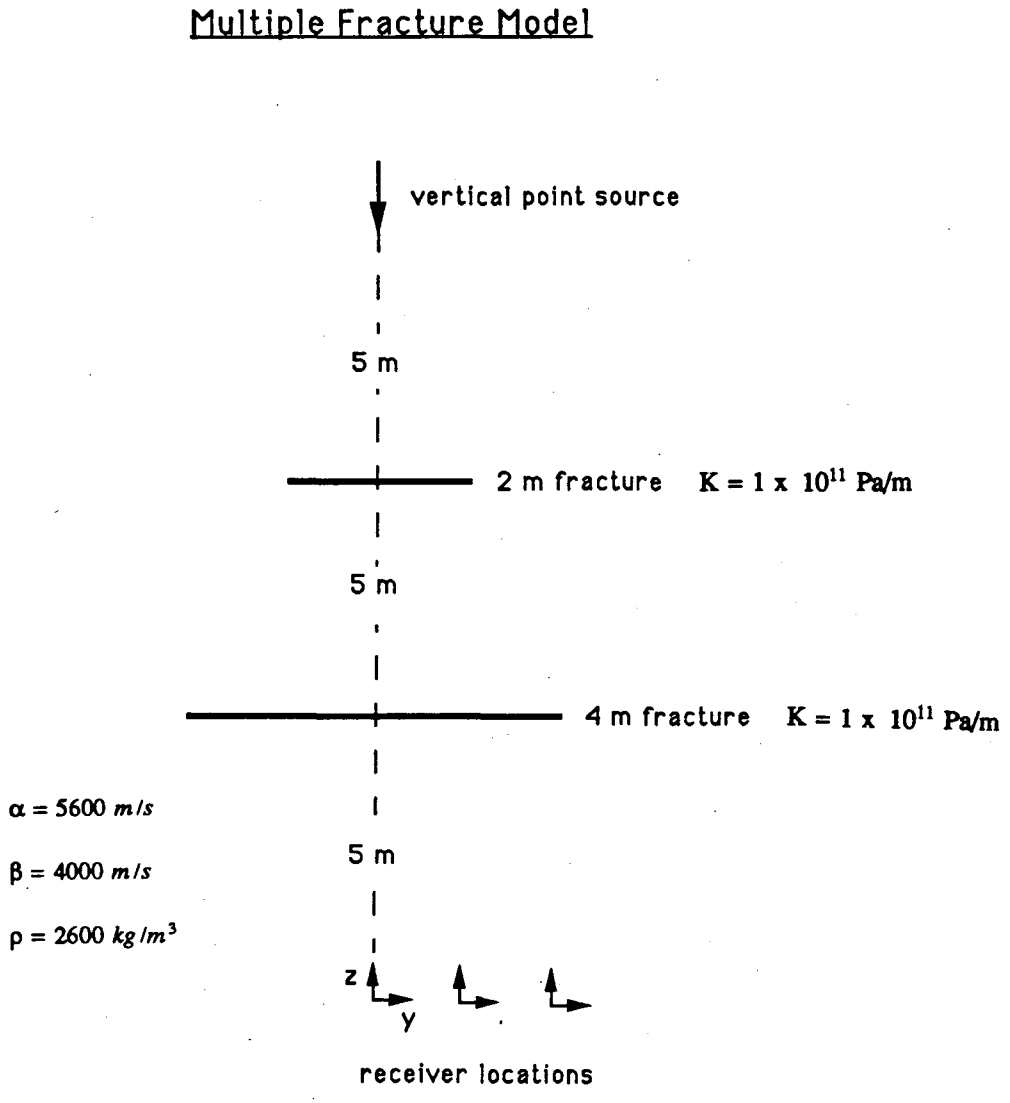

Figure 3.17 Multiple fracture model used to generate the synthetics in Figure 3.18.

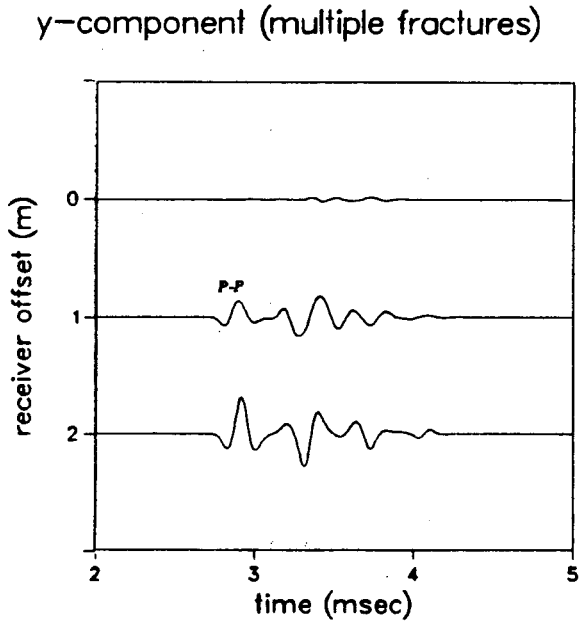

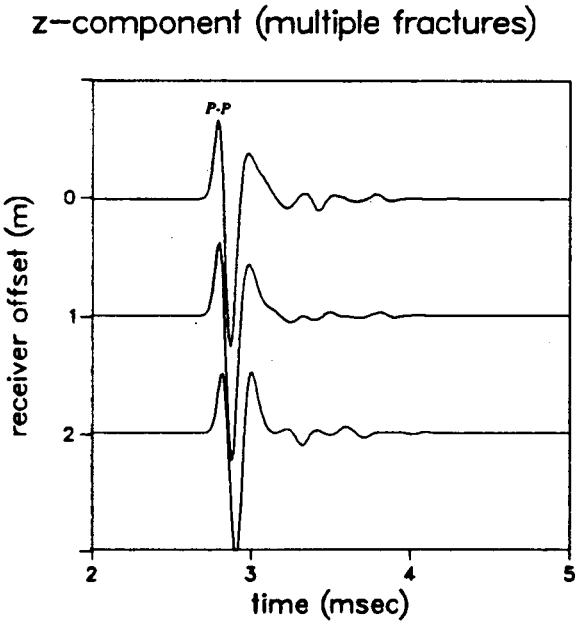

Figure 3.18 Kirchhoff transmission synthetics for the multiple fracture model shown in Figure 3.17.

stiffness fracture is to attenuate and remove high frequencies.

The last section outlined an multiple Kirchhoff integral approach for modeling wave transmission through multiple fractures. The use of multiple Kirchhoff integrals is valid only when the fractures are separated by many seismic wavelengths. This approach becomes computationally intensive when the number of fractures is increased and if multiple scattering between fractures is included.

CHAPTER 4

CONCLUSIONS AND RECOMMENDATIONS FOR FURTHER STUDY

This thesis has investigated the application of the Kirchhoff method to the problem of modeling elastic waves in fractured rock. It was shown that the Kirchhoff method is capable of modeling transmitted, reflected, and diffracted elastic waves from 3-dimensional fractures. This was accomplished by replacing the standard plane wave reflection and transmission coefficients for a welded contact between two elastic half-spaces by those for a non-welded contact described by the displacement discontinuity model.

It was demonstrated that the presence of a fracture produces converted waves and diffracted waves from the fracture edges. The amplitude and frequency content of these waves are controlled by the stiffness of the fracture and angles of incidence and reflection or refraction. If the stiffness varies randomly along the fracture surface, scattered waves will also be produced.

This study has presented only a very limited analysis of the interaction of an elastic wave with a fracture. A detailed analysis of this problem is not possible largely because of the limitations of the elastic Kirchhoff method. Reflection results were avoided because of the inaccuracies that result for small source-receiver offsets (Section 3.3). Multiple fracture results were limited to a simple example because of the computation time required to model more than several extensive fracture surfaces.

Only a very qualitative assessment of the accuracy of the elastic Kirchhoff method was made. To quantitatively examine the accuracy of the method would require the development of an exact solution using, for example, the boundary integral equation method (BIEM). With an exact solution, the utility of the Kirchhoff method for a variety of problem geometries could be fully explored.

The utility of the Kirchhoff method for modeling wave propagation in fractured rock lies in its ability to model scattering and diffraction from 3-dimensional fractures with varying properties (e.g., stiffness, topography). For very extensive, uniform fractures, no advantages are gained by using the Kirchhoff method and more computationally economical results can be obtained using ray and propagator matrix methods.

It would have been of interest to examine the effects of fluid-filled fractures since they are pervasive in many areas of geological importance (e.g., geothermal and oil fields). A detailed study of the effects of P and S waves in a fluid-filled fractures may reveal waveform signatures that are unique to fluid-filled fractures. This could have direct implications in the problem of discriminating between dry and fluid-filled fractures (Palmer, 1982).

This study focused primarily on presenting an approach for modeling elastic waves in fractured rock. Of more fundamental importance is the inverse problem of locating and characterizing fractures from observations of transmitted, reflected, and diffracted waves. The implications of this study are that inverse methods that incorporate amplitude information of reflected, transmitted, and scattered waves (e.g., diffraction tomography, Born inversion) are desirable for detecting and characterizing fractures.

REFERENCES

Achenbach, J. D., A. K. Gautesen, and H. McMaken (1982). Ray Methods for Waves in Elastic Solids, Pittman Publishing Inc., Massachusetts.

Aki, K. and P. G. Richards (1980). Quantitative Seismology, vol. I, W. H. Freeman and Co., New York.

Aki, K., M. Fehler, R. L. Aamodt, J. N. Albright, R. M. Potter, C. M. Pearson, and J. W. Tester (1982). Interpretation of seismic data from hydraulic fracturing experiments at the Fenton Hill, New Mexico, Hot Dry Rock geothermal site, J. Geophys. Res, 87, 936-944.

Baker, B. B. and E. T. Copson (1950). The mathematical theory of Huygen's principle, Clarendon Press, Oxford.

Bleistein, N. (1982). Mathematical Methods for Wave Phenomena, Academic Press Inc., London.

Bleistein, N. (1986). Two-and-one-half dimensional in-plane wave propagation, Geophys. Prosp., 34, 696-703.

Buck, O., D. K. Rehbein, and R. B. Thompson (1987). Crack tip shielding by asperity contact as determined by acoustic measurements, Engin. Frac. Mech., 28, 413-424.

Carswell, A. and W. M. Moon (1989). Application of multioffset vertical seismic profiling in fracture mapping, Geophysics, 54, 737-746.

Chatterjee, A. K. and A. K. Mal (1978). Elastic moduli of two-component systems, J. Geophys. Res., 85, 1785-1792.

Cohen, J. (1988). Asymptotic elastic Green's tensor, Geophysics, 53, 992-994.

Cole, D. M. (1980). A numerical boundary integral equation method for transient motions, PhD Thesis, California Institute of Technology.

Crampin, S. (1981). A review of wave motion in anisotropic and cracked elastic-media, Wave Motion, 3, 343-391.

Dalton, D. and M. J. Yedlin (1988). Exact modeling of acoustic diffraction by a half-plane, Expanded Abstracts, SEG 58th Annual Inter. Meeting and Exposition, 1988, 1039-1042.

Deregowski, S. M. and S. M. Brown (1983). A theory of acoustic diffractors applied to 2-D models, Geophys. Prosp., 31, 293-333.

Dmowska, R. and J. R. Rice (1983). Fracture theory and its seismological implications, Elsevier Publishing Co./Polish Scientific Publishers.

Fehler, M. (1982). Using dual-well seismic measurements to infer the mechanical properties of a hot dry rock geothermal system, J. Geophys. Res., 87, 5485-5494.

Fehler, M. and C. Pearson (1984). Cross-hole seismic surveys: application for studying subsurface fracture systems at a hot dry rock geothermal site, Geophysics, 49, 37-48.

Frankel, A. and R. W. Clayton (1986). Finite difference simulations of seismic scattering: implications for the propagation of short-period seismic waves in the crust and models of crustal heterogeneity, J. Geophys. Res., 91, 6465-6489.

Frazer, L. N. and M. K. Sen (1985). Kirchhoff-Helmholtz reflection seismograms in a laterally inhomogeneous multi-layered elastic medium - I. Theory, Geophys, J. R. astr. Soc., 80, 121-147.

Frazer, L. N. (1987). Multifold path integral synthetic seismograms, I. Theory, Geophys. J. R. astr. Soc.,

88, 621-646.

Green, A. G. and J. A. Mair (1982). Subhorizontal fractures in a granitic pluton: Their detection and implications for radioactive waste disposal, Geophysics, 48, 1428-1449.

Haddon, R. A. W. and P. W. Buchen (1981). Use of Kirchhoff's formula for body wave calculations in the earth, Geophys. J. R. astr. Soc., 67, 587-598.

Hardin, E. L., C. H. Cheng, F. L. Paillet, and J. D. Mendelson (1987). Fracture characterization by means of attenuation and generation of tube waves in fractured crystalline rock at Mirror Lake, New Hampshire, J. Geophys. Res., 92, 7989-8006.

Hilterman, F. J. (1970). Three-dimensional seismic modeling, Geophysics, 35, 1020-1037.

Hilterman, F. J. (1975). Amplitudes of seismic waves - a quick look, Geophysics, 40, 745-762.

Hudson, J. A. (1981). Wave speeds and attenuation of elastic waves in material containing cracks, Geophys. J. R. astr. Soc., 64, 133-150.

Jebsen, G. M. and H. Medwin (1982). On the failure of the Kirchhoff assumption in backscatter, J. Acoust. Soc. Am., 72, 1607-1611.

Johnson, L. R. (1974). Green's function for Lamb's problem, Geophy. J. R. astr. Soc., 37, 99-131.

Kuo, J. T. and T. F. Dai (1984). Kirchhoff elastic wave migration for the case of noncoincident source and receiver, Geophysics, 49, 1223-1238.

LeBras, R. and R. W. Clayton (1988). An iterative inversion of back-scattered acoustic waves, Geophysics, 53, 501-508.

Majer, E. L., J. E. Peterson, T. V. McEvilly, and J. C. S. Long (1986). VSP/Tomographic studies for fracture detection and characterization, LBL Annual Report, Earth Sciences Division, 1986, 230-233.

Majer, E. L., J. E. Peterson, and J. C. S. Long (1987). Controlled seismic cross-hole experiments for fracture characterization, LBL Annual Report, Earth Sciences Division, 1987, 114-117.

Majer, E. L., T. V. McEvilly, F. S. Eastwood, and L. R. Myer (1988). Fracture detection using P-wave and S-wave vertical seismic profiling at The Geysers, Geophysics, 53, 76-84.

Mal, A. K. (1982). Final technical report on project scattering of elastic waves, Lawrence Livermore Laboratory, UCRL-15501.

Palmer, S. P. (1982). Fracture detection in crystalline rock using ultrasonic reflection techniques, PhD Thesis, University of California, Berkeley.

Pao, Y. H. and C. C. Mow (1973). Diffraction of elastic waves and dynamic stress concentrations, Crane Russak and Co., New York.

Pao, Y. H. and V. Varatharajulu (1976). Huygens' principle, radiation conditions, and integral formulas for the scattering of elastic waves, J. Acoust. Soc. Am., 59, 1361-1371.

Paul, A. and M. Campillo (1988). Diffraction and conversion of elastic waves at a corrugated interface, Geophysics,53, 1415-1424.

Pratt, R. G. and M. H. Worthington (1988). The application of diffraction tomography to cross-hole seismic data, Geophysics, 53, 1284-1294.

Pyrak, L. J. (1988). Seismic visibility of fractures, PhD Thesis, University of California, Berkeley.

Rayleigh, L. (1945). The Theory of Sound, 2nd Edition, Dover Publications, New York.

Schuster, G. T. and L. C. Smith (1985). A comparison among four direct boundary integral methods, J. Acoust. Soc. Am., 77, 850-864.

Scott, P. (1985). Application of the Kirchhoff-Helmholtz integral to problems in body wave seismology, PhD Thesis, California Institute of Technology.

Sen, M. K. and L. N. Frazer (1985). Kirchhoff-Helmholtz reflection seismograms in a laterally inhomogeneous multi-layered elastic medium - II. Computations, Geophys, J. R. astr. Soc., 82, 415-437.

Sen, M. K. and L. N. Frazer (1987). Synthetic seismograms using multifold path integrals, II. Computations, Geophys. J. R. astr. Soc., 88, 647-671.

Shoenberg, M. (1980). Elastic wave behavior across linear slip interfaces, J. Acoust. Soc. Am., 68, 1516-1521.

Shoenberg, M. (1983). Reflection of elastic waves from periodically stratified media with interfacial slip, Geophys. Prosp., 31, 265-292.

Stewart, R. R., R. M. Turpening, M. N. Toksoz (1981). Study of a subsurface fracture zone by vertical seismic profiling, Geophys. Res. Let., 8, 1132-1135.

Suarez, F. R., L. J. Pyrak-Nolte, N. G. W. Cook, F. Doyle, and L. R. Myer (1988). Transmission of S-waves across a thin liquid layer, LBL Annual Report, Earth Science Division, 1988, 34-37.

Sullivan, M. F. (1987). Prestack Kirchhoff inversion and modeling in 2.5 dimensions, PhD Thesis, Colorado School of Mines.

Sumner, B. (1988). Asymptotic Solutions to forward and Inverse Problems in Isotropic Elastic Media, PhD Thesis, Colorado School of Mines.

Thorsos, E. I. (1988). The validity of the Kirchhoff approximation for rough surface scattering using a Gaussian roughness spectrum, J. Acoust. Soc. Am., 83, 78-92.

Trorey, A. W. (1970). A simple theory for seismic diffractions, Geophysics, 35, 762-784.

Trorey, A. W. (1977). Diffractions for arbitrary source-receiver locations, Geophysics, 42, 1177-1182.

Wirgin, A. (1989). Scattering from hard and soft corrugated surfaces: iterative corrections to the Kirchhoff approximation through the extinction theorem, J. Acoust. Soc. Am., 85, 670-679.

Wong, J., P. Hurley, and G. F. West (1983). Crosshole seismology and seismic imaging in crystalline rocks, Geophys. Res. Let., 10, 686-689.

Wu, R. and M. N. Toksoz (1987). Diffraction tomography and multisource holography applied to seismic imaging, Geophysics, 52, 11-25.

APPENDIX A

```
      program kirch25d
c
#include "common.f"
c
ccccccccccccccccccccccccccccccccccccccccccccccccccccccccccccccccc
c
c  Version: 3/20/89
c
c  Program KIRCH25D solves the frequency domain, elastic
c  Kirchhoff integral for a single 2.5D fracture.  The
c  medium is assumed to be homogeneous and isotropic.
c
c  This version is set up for transmission through a fracture.
c  To compute the reflected wavefield, redefine theta(j,2)
c  in subroutine DIRCOS to:
c
c   theta(j,2)=acos(an(j)*gam(1)+bn(j)*gam(2)+cn(j)*gam(3))
c
c
c  References:
c
c    Pao,Y. H and V. Varatharajulu (1976).  Huygens'
c      principle, radiation conditions, and integral
c      formulas for the scattering of elastic waves,
c      J. Acoust. Soc. Am., v.59, 6, 1361-1371.
c
c    Sumner, B.L. (1988). Asymptotic solutions to
c      forward and inverse problems in isotropic
c      elastic media, PhD Thesis, Colorado School
c      of Mines.
c
ccccccccccccccccccccccccccccccccccccccccccccccccccccccccccccccccc
c
c *Dimension arrays:
      dimension ur1(nstp),ur2(nstp),ur3(nstp),ui1(nstp),ui2(nstp),
     $ui3(nstp)
      complex u1,u2,u3
c
c *Open files:
c
      open(unit=1,file='xyz.out',status='unknown')
      open(unit=2,file='xyzi.out',status='unknown')
c
c *Read problem info.:
c
      call rdata
      write(1,*) nstep
      write(2,*) nstep
c
c *Evaluate the Kirchhoff integral:
c
      fmax=nstep/tmax
      fstep=1./tmax
      wstep=2.*pi*fstep
```

```
      tstep=tmax/nstep
      nfreq=nstep/2
c
c .. loop over frequency:
      do i=1,nfreq+1
        u1=cmplx(0.,0.)
        u2=cmplx(0.,0.)
        u3=cmplx(0.,0.)
        w=wstep*float(i-1)
c
c .. loop over surface elements:
        do j=1,nelem
c
          if(i.eq.1)then
           rsk(j)=((xk(j)-xs)**2.+(yk(j)-ys)**2.+(zk(j)-zs)**2.)**.5
              rrk(j)=((xk(j)-x)**2.+(yk(j)-y)**2.+(zk(j)-z)**2.)**.5
          endif
c
c .. calculate direction cosines:
          call dircos(j)
          psi(j,1)=theta(j,1)
          psi(j,2)=theta(j,2)
c
c .. calculate stiffness transmission coefficients:
          call shoenberg(j)
c
c .. set up displacement vector and stress tensor:
          call distress(j,i)
c
c .. set up Green's displacement tensor:
          call gtensor(j)
c
c .. set up Green's stress tensor:
          call stensor(j)
c
c  Calculate the 3-components of displacement:
c
c .. PP inner product:
          call inpp(j)
c
c .. SS inner product:
          call inss(j)
c
c .. PS inner product:
          call inps(j)
c
c .. SP inner product:
          call insp(j)
c
c .. SH inner product:
          call insh(j)
c
c .. add inner products:
          do imod=1,5
```

```
            u1=(ntg(imod,1)-uns(imod,1))*surf(j)+u1
            u2=(ntg(imod,2)-uns(imod,2))*surf(j)+u2
            u3=(ntg(imod,3)-uns(imod,3))*surf(j)+u3
          enddo
c
        enddo
c
c .. store displacement:
        ur1(i)=real(u1)
        ui1(i)=aimag(u1)
        ur2(i)=real(u2)
        ui2(i)=aimag(u2)
        ur3(i)=real(u3)
        ui3(i)=aimag(u3)
c
c .. complex conjugate:
        ur1(nstep+2-i)=ur1(i)
        ui1(nstep+2-i)=-ui1(i)
        ur2(nstep+2-i)=ur2(i)
        ui2(nstep+2-i)=-ui2(i)
        ur3(nstep+2-i)=ur3(i)
        ui3(nstep+2-i)=-ui3(i)
c
      enddo
c
c  Fourier Transform displacement to time-domain:
      call fastf(nstep,ur1,ui1)
      call fastf(nstep,ur2,ui2)
      call fastf(nstep,ur3,ui3)
      t=0.
      do k=1,nstep
        t=tstep*float(k-1)
        write(1,*) t,ur1(k),ur2(k),ur3(k)
        write(2,*) t,ui1(k),ui2(k),ui3(k)
      enddo
c
      end
c
c
      common.f
      parameter (maxel=35344,nstp=1024,pi=3.14159265)
      common /main/ rrk(maxel),rsk(maxel),wstep,w
      complex tpp,tps,tss,tsp,tsh
      common /transm/ theta(maxel,2),psi(maxel,2),
     $tpp,tps,tss,tsp,tsh
      complex f(nstp)
      real lamb
      common /rdata/ dens,bmod,smod,cp,cs,tmax,nstep,
     $stifn,stift,x,y,z,xs,ys,zs,itype,ntrsf,f,
     $nelem,xk(maxel),yk(maxel),zk(maxel),an(maxel),
     $bn(maxel),cn(maxel),lamb,surf(maxel)
      complex up(3),us(3),uh(3),tlmp(3,3),tlms(3,3),tlmh(3,3),
     $gmnp(3,3),gmns(3,3),slmnp(3,3,3),slmns(3,3,3)
      common /distre/ up,us,uh,tlmp,tlms,tlmh,gmnp,gmns,slmnp,slmns
```

```
      common /dircos/ gama(3),gam(3),gasv(3),gash(3),gapt(3)
      complex ntg(5,3),uns(5,3)
      common /inner/ ntg,uns
c
c
      subroutine dircos(j)
c
#include "common.f"
c
c  Subroutine computes the direction cosines.
c
c .. compute Rs direction cosines:
      gama(1)=(xk(j)-xs)/rsk(j)
      gama(2)=(yk(j)-ys)/rsk(j)
      gama(3)=(zk(j)-zs)/rsk(j)
c
c .. compute R direction cosines:
      gam(1)=(x-xk(j))/rrk(j)
      gam(2)=(y-yk(j))/rrk(j)
      gam(3)=(z-zk(j))/rrk(j)
c
c .. compute angles of incidence and refraction:
      theta(j,1)=acos(-an(j)*gama(1)-bn(j)*gama(2)-cn(j)*gama(3))
      theta(j,2)=acos(-an(j)*gam(1)-bn(j)*gam(2)-cn(j)*gam(3))
c
c .. compute SH direction cosines:
      if (theta(j,1).eq.0) theta(j,1)=1.e-29
      gash(1)=(cn(j)*gama(2)-bn(j)*gama(3))/sin(theta(j,1))
      gash(2)=(an(j)*gama(3)-cn(j)*gama(1))/sin(theta(j,1))
      gash(3)=(bn(j)*gama(1)-an(j)*gama(2))/sin(theta(j,1))
c
c .. compute SV direction cosines:
      gasv(1)=gash(2)*gama(3)-gash(3)*gama(2)
      gasv(2)=gash(3)*gama(1)-gash(1)*gama(3)
      gasv(3)=gash(1)*gama(2)-gash(2)*gama(1)
c
      return
      end
c
c
      subroutine distress(j,im)
c
#include "common.f"
c
c  This subroutine calculates the surface stresses and displacements
c  generated by an incident P or S wave.
c
c  Dimension arrays:
      complex ep,es,cep,ces,fp,fsv,fsh,cmup,cmus
c
c  Source function and displacements:
      term=1./(4.*pi*dens*rsk(j))
      cp2=cp**2.
      cs2=cs**2.
```

```
      pt=rsk(j)/cp
      st=rsk(j)/cs
      ep=cmplx(0.,w*pt)
      es=cmplx(0.,w*st)
      cep=cexp(ep)
      ces=cexp(es)
c
      do i=1,3
        fp=f(im)*gapt(i)*gama(i)
        fsv=f(im)*gapt(i)*gasv(i)
        fsh=f(im)*gapt(i)*gash(i)
        up(i)=term*gama(i)*fp*cep/cp2
        us(i)=term*gasv(i)*fsv*ces/cs2
        uh(i)=term*gash(i)*fsh*ces/cs2
      enddo
c
c  Stresses:
      cmup=cmplx(0.,w/cp)
      tlmp(1,1)=-cmup*(lamb*(up(1)*gama(1)+up(2)*gama(2)+
     $          up(3)*gama(3))+2.*smod*up(1)*gama(1))
      tlmp(1,2)=-cmup*smod*(up(1)*gama(2)+up(2)*gama(1))
      tlmp(1,3)=-cmup*smod*(up(1)*gama(3)+up(3)*gama(1))
      tlmp(2,1)=tlmp(1,2)
      tlmp(2,2)=-cmup*(lamb*(up(1)*gama(1)+up(2)*gama(2)+
     $          up(3)*gama(3))+2.*smod*up(2)*gama(2))
      tlmp(2,3)=-cmup*smod*(up(2)*gama(3)+up(3)*gama(2))
      tlmp(3,1)=tlmp(1,3)
      tlmp(3,2)=tlmp(2,3)
      tlmp(3,3)=-cmup*(lamb*(up(1)*gama(1)+up(2)*gama(2)+
     $          up(3)*gama(3))+2.*smod*up(3)*gama(3))
c
      cmus=cmplx(0.,w/cs)
      tlms(1,1)=-cmus*2.*smod*us(1)*gama(1)
      tlms(1,2)=-cmus*smod*(us(1)*gama(2)+us(2)*gama(1))
      tlms(1,3)=-cmus*smod*(us(1)*gama(3)+us(3)*gama(1))
      tlms(2,1)=tlms(1,2)
      tlms(2,2)=-cmus*2.*smod*us(2)*gama(2)
      tlms(2,3)=-cmus*smod*(us(2)*gama(3)+us(3)*gama(2))
      tlms(3,1)=tlms(1,3)
      tlms(3,2)=tlms(2,3)
      tlms(3,3)=-cmus*2.*smod*us(3)*gama(3)
c
      tlmh(1,1)=-cmus*2.*smod*uh(1)*gama(1)
      tlmh(1,2)=-cmus*smod*(uh(1)*gama(2)+uh(2)*gama(1))
      tlmh(1,3)=-cmus*smod*(uh(1)*gama(3)+uh(3)*gama(1))
      tlmh(2,1)=tlmh(1,2)
      tlmh(2,2)=-cmus*2.*smod*uh(2)*gama(2)
      tlmh(2,3)=-cmus*smod*(uh(2)*gama(3)+uh(3)*gama(2))
      tlmh(3,1)=tlmh(1,3)
      tlmh(3,2)=tlmh(2,3)
      tlmh(3,3)=-cmus*2.*smod*uh(3)*gama(3)
c
      return
      end
```

```
c
c
      subroutine fastf(n,fr,fi)
c
#include "common.f"
c
c from Kanasewich pp.59-60
c Note: This FFT routine is set up to compute the inverse transform.
c       The following FT sign convention is used:
c
c         f(w)=SUM [f(t)exp(-iwt)]
c         f(t)=(1/n)SUM [f(w)exp(+iwt)]
c
      dimension fr(nstp),fi(nstp)
c
      m=0
      kd=n
1     kd=kd/2
      m=m+1
      if(kd.ge.2)goto 1
      nd2=n/2
      nm1=n-1
      l=1
c
      do 4 k=1,nm1
      if (k.ge.l)goto 2
      gr=fr(l)
      gi=fi(l)
      fr(l)=fr(k)
      fi(l)=fi(k)
      fr(k)=gr
      fi(k)=gi
2     nnd2=nd2
3     if (nnd2.ge.l)goto 4
      l=l-nnd2
      nnd2=nnd2/2
      goto 3
4     l=l+nnd2
c
      do 6 j=1,m
      nj=2**j
      njd2=nj/2
      eu=1.
      ez=0.
      er=cos(-pi/njd2)
      ei=sin(-pi/njd2)
c
      do 6 it=1,njd2
      do 5 iw=it,n,nj
      iwj=iw+njd2
      gr=fr(iwj)*eu-fi(iwj)*ez
      gi=fi(iwj)*eu+fr(iwj)*ez
      fr(iwj)=fr(iw)-gr
      fi(iwj)=fi(iw)-gi
```

```
      fr(iw)=fr(iw)+gr
5     fi(iw)=fi(iw)+gi
      seu=eu
      eu=seu*er-ez*ei
6     ez=ez*er+seu*ei
c
c  divide by n:
      do in=1,n
        fr(in)=fr(in)/float(n)
        fi(in)=fi(in)/float(n)
      enddo
c
      return
      end
c
c
      subroutine gtensor(j)
c
#include "common.f"
c
c  This subroutine sets up the Green's displacement tensor.
c
      complex ep,es,cep,ces,cepp,cess
c
      if(w.eq.0)w=3.e-15
      gterm=1./(4.*pi*dens*w**2.*rrk(j))
      pk=w/cp
      sk=w/cs
      ep=cmplx(0.,pk*rrk(j))
      es=cmplx(0.,sk*rrk(j))
      cep=cexp(ep)
      ces=cexp(es)
      cepp=pk**2.*cep
      cess=sk**2.*ces
c
c  P-wave Green's displacement tensor:
      gmnp(1,1)=gterm*gam(1)**2.*cepp
      gmnp(1,2)=gterm*gam(1)*gam(2)*cepp
      gmnp(1,3)=gterm*gam(1)*gam(3)*cepp
      gmnp(2,1)=gmnp(1,2)
      gmnp(2,2)=gterm*gam(2)**2.*cepp
      gmnp(2,3)=gterm*gam(2)*gam(3)*cepp
      gmnp(3,1)=gmnp(1,3)
      gmnp(3,2)=gmnp(2,3)
      gmnp(3,3)=gterm*gam(3)**2.*cepp
c
c  S-wave Green's displacement tensor:
      gmns(1,1)=gterm*(1.-gam(1)**2.)*cess
      gmns(1,2)=-gterm*gam(1)*gam(2)*cess
      gmns(1,3)=-gterm*gam(1)*gam(3)*cess
      gmns(2,1)=gmns(1,2)
      gmns(2,2)=gterm*(1.-gam(2)**2.)*cess
      gmns(2,3)=-gterm*gam(2)*gam(3)*cess
      gmns(3,1)=gmns(1,3)
```

```
      gmns(3,2)=gmns(2,3)
      gmns(3,3)=gterm*(1.-gam(3)**2.)*cess
c
      return
      end
c
c
      subroutine inpp(j)
c
#include "common.f"
c
c  Subroutine does the PP t*G and u*S inner products:
c
      complex a1,a2,a3,b(9),cex,cmult
c
c .. 2.5d multiplier
      cex=cmplx(0.,pi/4.)
      cmult=(cp*2.*pi/abs(w)*rsk(j)*rrk(j)/(rsk(j)+rrk(j)))**.5*
     $     cexp(cex)
c
c .. compute n*t*G
      a1=an(j)*tlmp(1,1)+bn(j)*tlmp(2,1)+cn(j)*tlmp(3,1)
      a2=an(j)*tlmp(1,2)+bn(j)*tlmp(2,2)+cn(j)*tlmp(3,2)
      a3=an(j)*tlmp(1,3)+bn(j)*tlmp(2,3)+cn(j)*tlmp(3,3)
      ntg(1,1)=cmult*tpp*(a1*gmnp(1,1)+a2*gmnp(2,1)+a3*gmnp(3,1))
      ntg(1,2)=cmult*tpp*(a1*gmnp(1,2)+a2*gmnp(2,2)+a3*gmnp(3,2))
      ntg(1,3)=cmult*tpp*(a1*gmnp(1,3)+a2*gmnp(2,3)+a3*gmnp(3,3))
c
c .. compute u*(n*S)
      b(1)=an(j)*slmnp(1,1,1)+bn(j)*slmnp(2,1,1)+cn(j)*slmnp(3,1,1)
      b(2)=an(j)*slmnp(1,1,2)+bn(j)*slmnp(2,1,2)+cn(j)*slmnp(3,1,2)
      b(3)=an(j)*slmnp(1,1,3)+bn(j)*slmnp(2,1,3)+cn(j)*slmnp(3,1,3)
      b(4)=an(j)*slmnp(1,2,1)+bn(j)*slmnp(2,2,1)+cn(j)*slmnp(3,2,1)
      b(5)=an(j)*slmnp(1,2,2)+bn(j)*slmnp(2,2,2)+cn(j)*slmnp(3,2,2)
      b(6)=an(j)*slmnp(1,2,3)+bn(j)*slmnp(2,2,3)+cn(j)*slmnp(3,2,3)
      b(7)=an(j)*slmnp(1,3,1)+bn(j)*slmnp(2,3,1)+cn(j)*slmnp(3,3,1)
      b(8)=an(j)*slmnp(1,3,2)+bn(j)*slmnp(2,3,2)+cn(j)*slmnp(3,3,2)
      b(9)=an(j)*slmnp(1,3,3)+bn(j)*slmnp(2,3,3)+cn(j)*slmnp(3,3,3)
      uns(1,1)=cmult*tpp*(b(1)*up(1)+b(4)*up(2)+b(7)*up(3))
      uns(1,2)=cmult*tpp*(b(2)*up(1)+b(5)*up(2)+b(8)*up(3))
      uns(1,3)=cmult*tpp*(b(3)*up(1)+b(6)*up(2)+b(9)*up(3))
c
      return
      end
c
c
      subroutine inps(j)
c
#include "common.f"
c
c  Subroutine computes the PS t*G and u*S inner products:
c
      complex a1,a2,a3,b(9),cex,cmult
c
```

```
c .. 2.5d multiplier
      cex=cmplx(0.,pi/4.)
      cmult=(2.*pi/abs(w)*cp*rsk(j)*cs*rrk(j)/(cp*rsk(j)+
     $     cs*rrk(j)))**.5*cexp(cex)
c
c .. compute n*t*G
      a1=an(j)*tlmp(1,1)+bn(j)*tlmp(2,1)+cn(j)*tlmp(3,1)
      a2=an(j)*tlmp(1,2)+bn(j)*tlmp(2,2)+cn(j)*tlmp(3,2)
      a3=an(j)*tlmp(1,3)+bn(j)*tlmp(2,3)+cn(j)*tlmp(3,3)
      ntg(3,1)=cmult*tps*(a1*gmns(1,1)+a2*gmns(2,1)+a3*gmns(3,1))
      ntg(3,2)=cmult*tps*(a1*gmns(1,2)+a2*gmns(2,2)+a3*gmns(3,2))
      ntg(3,3)=cmult*tps*(a1*gmns(1,3)+a2*gmns(2,3)+a3*gmns(3,3))
c
c .. compute u*(n*S)
      b(1)=an(j)*slmns(1,1,1)+bn(j)*slmns(2,1,1)+cn(j)*slmns(3,1,1)
      b(2)=an(j)*slmns(1,1,2)+bn(j)*slmns(2,1,2)+cn(j)*slmns(3,1,2)
      b(3)=an(j)*slmns(1,1,3)+bn(j)*slmns(2,1,3)+cn(j)*slmns(3,1,3)
      b(4)=an(j)*slmns(1,2,1)+bn(j)*slmns(2,2,1)+cn(j)*slmns(3,2,1)
      b(5)=an(j)*slmns(1,2,2)+bn(j)*slmns(2,2,2)+cn(j)*slmns(3,2,2)
      b(6)=an(j)*slmns(1,2,3)+bn(j)*slmns(2,2,3)+cn(j)*slmns(3,2,3)
      b(7)=an(j)*slmns(1,3,1)+bn(j)*slmns(2,3,1)+cn(j)*slmns(3,3,1)
      b(8)=an(j)*slmns(1,3,2)+bn(j)*slmns(2,3,2)+cn(j)*slmns(3,3,2)
      b(9)=an(j)*slmns(1,3,3)+bn(j)*slmns(2,3,3)+cn(j)*slmns(3,3,3)
      uns(3,1)=cmult*tps*(b(1)*up(1)+b(4)*up(2)+b(7)*up(3))
      uns(3,2)=cmult*tps*(b(2)*up(1)+b(5)*up(2)+b(8)*up(3))
      uns(3,3)=cmult*tps*(b(3)*up(1)+b(6)*up(2)+b(9)*up(3))
c
      return
      end
c
c
      subroutine insh(j)
c
#include "common.f"
c
c  Subroutine computes the SHSH t*G and u*S inner products:
c
      complex a1,a2,a3,b(9),cex,cmult
c
c .. 2.5d multiplier
      cex=cmplx(0.,pi/4.)
      cmult=(cs*2.*pi/abs(w)*rsk(j)*rrk(j)/(rsk(j)+rrk(j)))**.5*
     $     cexp(cex)
c
c .. compute n*t*G
      a1=an(j)*tlmh(1,1)+bn(j)*tlmh(2,1)+cn(j)*tlmh(3,1)
      a2=an(j)*tlmh(1,2)+bn(j)*tlmh(2,2)+cn(j)*tlmh(3,2)
      a3=an(j)*tlmh(1,3)+bn(j)*tlmh(2,3)+cn(j)*tlmh(3,3)
      ntg(5,1)=cmult*tsh*(a1*gmns(1,1)+a2*gmns(2,1)+a3*gmns(3,1))
      ntg(5,2)=cmult*tsh*(a1*gmns(1,2)+a2*gmns(2,2)+a3*gmns(3,2))
      ntg(5,3)=cmult*tsh*(a1*gmns(1,3)+a2*gmns(2,3)+a3*gmns(3,3))
c
c .. compute u*(n*S)
      b(1)=an(j)*slmns(1,1,1)+bn(j)*slmns(2,1,1)+cn(j)*slmns(3,1,1)
```

```
      b(2)=an(j)*slmns(1,1,2)+bn(j)*slmns(2,1,2)+cn(j)*slmns(3,1,2)
      b(3)=an(j)*slmns(1,1,3)+bn(j)*slmns(2,1,3)+cn(j)*slmns(3,1,3)
      b(4)=an(j)*slmns(1,2,1)+bn(j)*slmns(2,2,1)+cn(j)*slmns(3,2,1)
      b(5)=an(j)*slmns(1,2,2)+bn(j)*slmns(2,2,2)+cn(j)*slmns(3,2,2)
      b(6)=an(j)*slmns(1,2,3)+bn(j)*slmns(2,2,3)+cn(j)*slmns(3,2,3)
      b(7)=an(j)*slmns(1,3,1)+bn(j)*slmns(2,3,1)+cn(j)*slmns(3,3,1)
      b(8)=an(j)*slmns(1,3,2)+bn(j)*slmns(2,3,2)+cn(j)*slmns(3,3,2)
      b(9)=an(j)*slmns(1,3,3)+bn(j)*slmns(2,3,3)+cn(j)*slmns(3,3,3)
      uns(5,1)=cmult*tsh*(b(1)*uh(1)+b(4)*uh(2)+b(7)*uh(3))
      uns(5,2)=cmult*tsh*(b(2)*uh(1)+b(5)*uh(2)+b(8)*uh(3))
      uns(5,3)=cmult*tsh*(b(3)*uh(1)+b(6)*uh(2)+b(9)*uh(3))
c
      return
      end
c
c
      subroutine insp(j)
c
#include "common.f"
c
c  Subroutine computes the SP t*G and u*S inner products:
c
      complex a1,a2,a3,b(9),cex,cmult
c
c .. 2.5d multiplier
      cex=cmplx(0.,pi/4.)
      cmult=(2.*pi/abs(w)*cs*rsk(j)*cp*rrk(j)/(cs*rsk(j)+
     $      cp*rrk(j)))**.5*cexp(cex)
c
c .. compute n*t*G
      a1=an(j)*tlms(1,1)+bn(j)*tlms(2,1)+cn(j)*tlms(3,1)
      a2=an(j)*tlms(1,2)+bn(j)*tlms(2,2)+cn(j)*tlms(3,2)
      a3=an(j)*tlms(1,3)+bn(j)*tlms(2,3)+cn(j)*tlms(3,3)
      ntg(4,1)=cmult*tsp*(a1*gmnp(1,1)+a2*gmnp(2,1)+a3*gmnp(3,1))
      ntg(4,2)=cmult*tsp*(a1*gmnp(1,2)+a2*gmnp(2,2)+a3*gmnp(3,2))
      ntg(4,3)=cmult*tsp*(a1*gmnp(1,3)+a2*gmnp(2,3)+a3*gmnp(3,3))
c
c .. compute u*(n*S)
      b(1)=an(j)*slmnp(1,1,1)+bn(j)*slmnp(2,1,1)+cn(j)*slmnp(3,1,1)
      b(2)=an(j)*slmnp(1,1,2)+bn(j)*slmnp(2,1,2)+cn(j)*slmnp(3,1,2)
      b(3)=an(j)*slmnp(1,1,3)+bn(j)*slmnp(2,1,3)+cn(j)*slmnp(3,1,3)
      b(4)=an(j)*slmnp(1,2,1)+bn(j)*slmnp(2,2,1)+cn(j)*slmnp(3,2,1)
      b(5)=an(j)*slmnp(1,2,2)+bn(j)*slmnp(2,2,2)+cn(j)*slmnp(3,2,2)
      b(6)=an(j)*slmnp(1,2,3)+bn(j)*slmnp(2,2,3)+cn(j)*slmnp(3,2,3)
      b(7)=an(j)*slmnp(1,3,1)+bn(j)*slmnp(2,3,1)+cn(j)*slmnp(3,3,1)
      b(8)=an(j)*slmnp(1,3,2)+bn(j)*slmnp(2,3,2)+cn(j)*slmnp(3,3,2)
      b(9)=an(j)*slmnp(1,3,3)+bn(j)*slmnp(2,3,3)+cn(j)*slmnp(3,3,3)
      uns(4,1)=cmult*tsp*(b(1)*us(1)+b(4)*us(2)+b(7)*us(3))
      uns(4,2)=cmult*tsp*(b(2)*us(1)+b(5)*us(2)+b(8)*us(3))
      uns(4,3)=cmult*tsp*(b(3)*us(1)+b(6)*us(2)+b(9)*us(3))
c
      return
      end
c
```

```
c
      subroutine inss(j)
c
#include "common.f"
c
c  Subroutine computes the SS t*G and u*S inner products:
c
      complex a1,a2,a3,b(9),cex,cmult
c
c .. 2.5d multiplier
      cex=cmplx(0.,pi/4.)
      cmult=(cs*2.*pi/abs(w)*rsk(j)*rrk(j)/(rsk(j)+rrk(j)))**.5*
     $      cexp(cex)
c
c .. compute n*t*G
      a1=an(j)*tlms(1,1)+bn(j)*tlms(2,1)+cn(j)*tlms(3,1)
      a2=an(j)*tlms(1,2)+bn(j)*tlms(2,2)+cn(j)*tlms(3,2)
      a3=an(j)*tlms(1,3)+bn(j)*tlms(2,3)+cn(j)*tlms(3,3)
      ntg(2,1)=cmult*tss*(a1*gmns(1,1)+a2*gmns(2,1)+a3*gmns(3,1))
      ntg(2,2)=cmult*tss*(a1*gmns(1,2)+a2*gmns(2,2)+a3*gmns(3,2))
      ntg(2,3)=cmult*tss*(a1*gmns(1,3)+a2*gmns(2,3)+a3*gmns(3,3))
c
c .. compute u*(n*S)
      b(1)=an(j)*slmns(1,1,1)+bn(j)*slmns(2,1,1)+cn(j)*slmns(3,1,1)
      b(2)=an(j)*slmns(1,1,2)+bn(j)*slmns(2,1,2)+cn(j)*slmns(3,1,2)
      b(3)=an(j)*slmns(1,1,3)+bn(j)*slmns(2,1,3)+cn(j)*slmns(3,1,3)
      b(4)=an(j)*slmns(1,2,1)+bn(j)*slmns(2,2,1)+cn(j)*slmns(3,2,1)
      b(5)=an(j)*slmns(1,2,2)+bn(j)*slmns(2,2,2)+cn(j)*slmns(3,2,2)
      b(6)=an(j)*slmns(1,2,3)+bn(j)*slmns(2,2,3)+cn(j)*slmns(3,2,3)
      b(7)=an(j)*slmns(1,3,1)+bn(j)*slmns(2,3,1)+cn(j)*slmns(3,3,1)
      b(8)=an(j)*slmns(1,3,2)+bn(j)*slmns(2,3,2)+cn(j)*slmns(3,3,2)
      b(9)=an(j)*slmns(1,3,3)+bn(j)*slmns(2,3,3)+cn(j)*slmns(3,3,3)
      uns(2,1)=cmult*tss*(b(1)*us(1)+b(4)*us(2)+b(7)*us(3))
      uns(2,2)=cmult*tss*(b(2)*us(1)+b(5)*us(2)+b(8)*us(3))
      uns(2,3)=cmult*tss*(b(3)*us(1)+b(6)*us(2)+b(9)*us(3))
c
      return
      end
c
c
      subroutine rdata
c
#include "common.f"
c
      open(unit=5,file='kirchhoffe.inp',status='old')
      read(5,10)
      read(5,10) dens
      read(5,10) cp
      read(5,10) cs
      smod=cs**2.*dens
      bmod=cp**2.*dens-4./3.*smod
      lamb=bmod-2./3.*smod
      read(5,10) tmax
      read(5,15) nstep
```

```
      read(5,10) stifn
      read(5,10) stift
      read(5,10) x
      read(5,10) y
      read(5,10) z
      read(5,10) xs
      read(5,10) ys
      read(5,10) zs
      read(5,20) (gapt(i),i=1,3)
      read(5,15) ntrsf
      do i=1,ntrsf
        read(5,25) fr,fi
        f(i)=cmplx(fr,fi)
      enddo
      read(5,15) nelem
      do i=1,nelem
        read(5,20) xk(i),yk(i),zk(i),an(i),bn(i),cn(i),surf(i)
      enddo
c
10    format(10x,e10.4)
15    format(10x,i10)
20    format(7e10.4)
25    format(2e15.9)
c
      return
      end
c
c
      subroutine shoenberg(ijk)
c
#include "common.f"
c
c  This subroutine computes transmission coefficients for a
c displacement discontinuity by inverting Shoenberg's A-matrix
c via Cramer's rule.  The following transmission coefficients
c are calculated:
c
c   (1) SH transmission coeff. (incident SH-wave)
c   (2) P & SV transmission coeff.'s (incident P-wave)
c   (3) P & SV transmission coeff.'s (incident SV-wave)
c
c
      dimension b(4)
      complex a(4,4),c(4,4)
c
      g1=2.*dens*cs*sin(psi(ijk,1))
      g2=2.*dens*cs*sin(psi(ijk,2))
      p1=dens*cp-g1*sin(theta(ijk,1))
      p2=dens*cp-g2*sin(theta(ijk,2))
      q1=dens*cs*(cos(psi(ijk,1)))**2.-.5*g1*sin(psi(ijk,1))
      q2=dens*cs*(cos(psi(ijk,2)))**2.-.5*g2*sin(psi(ijk,2))
c
c Shoenberg's stiffness matrix has the form: ax=b
c
```

```
      a(1,1)=cmplx(-p1,0.)
      a(2,1)=cmplx(g1*cos(theta(ijk,1)),0.)
      a(3,1)=cmplx(-sin(theta(ijk,1)),0.)
      a(4,1)=cmplx(cos(theta(ijk,1)),0.)
      a(1,2)=cmplx(g1*cos(theta(ijk,1)),0.)
      a(2,2)=cmplx(q1,0.)
      a(3,2)=cmplx(-cos(psi(ijk,1)),0.)
      a(4,2)=cmplx(-sin(psi(ijk,1)),0.)
      a(1,3)=cmplx(p2,0.)
      a(2,3)=cmplx(g2*cos(theta(ijk,2)),0.)
      a(3,3)=cmplx(sin(theta(ijk,2)),-w/stift*g2*cos(theta(ijk,2)))
      a(4,3)=cmplx(cos(theta(ijk,2)),-w/stifn*p2)
      a(1,4)=cmplx(g2*cos(psi(ijk,2)),0.)
      a(2,4)=cmplx(-q2,0.)
      a(3,4)=cmplx(-cos(psi(ijk,2)),w/stift*q2)
      a(4,4)=cmplx(sin(psi(ijk,2)),-w/stifn*g2*cos(psi(ijk,2)))
c
c  Cofactors needed to calculate the P-wave transmission coeff.:
c
      c(1,1)=a(2,2)*(a(3,3)*a(4,4)-a(4,3)*a(3,4))-
     $       a(2,3)*(a(3,2)*a(4,4)-a(4,2)*a(3,4))+
     $       a(2,4)*(a(3,2)*a(4,3)-a(4,2)*a(3,3))
      c(2,1)=-a(1,2)*(a(3,3)*a(4,4)-a(4,3)*a(3,4))+
     $       a(1,3)*(a(3,2)*a(4,4)-a(4,2)*a(3,4))-
     $       a(1,4)*(a(3,2)*a(4,3)-a(4,2)*a(3,3))
      c(3,1)=a(1,2)*(a(2,3)*a(4,4)-a(4,3)*a(2,4))-
     $       a(1,3)*(a(2,2)*a(4,4)-a(4,2)*a(2,4))+
     $       a(1,4)*(a(2,2)*a(4,3)-a(4,2)*a(2,3))
      c(4,1)=-a(1,2)*(a(2,3)*a(3,4)-a(3,3)*a(2,4))+
     $       a(1,3)*(a(2,2)*a(3,4)-a(3,2)*a(2,4))-
     $       a(1,4)*(a(2,2)*a(3,3)-a(3,2)*a(2,3))
      c(1,3)=a(2,1)*(a(3,2)*a(4,4)-a(4,2)*a(3,4))-
     $       a(2,2)*(a(3,1)*a(4,4)-a(4,1)*a(3,4))+
     $       a(2,4)*(a(3,1)*a(4,2)-a(4,1)*a(3,2))
      c(2,3)=-a(1,1)*(a(3,2)*a(4,4)-a(4,2)*a(3,4))+
     $       a(1,2)*(a(3,1)*a(4,4)-a(4,1)*a(3,4))-
     $       a(1,4)*(a(3,1)*a(4,2)-a(4,1)*a(3,2))
      c(3,3)=a(1,1)*(a(2,2)*a(4,4)-a(4,2)*a(2,4))-
     $       a(1,2)*(a(2,1)*a(4,4)-a(4,1)*a(2,4))+
     $       a(1,4)*(a(2,1)*a(4,2)-a(4,1)*a(2,2))
      c(4,3)=-a(1,1)*(a(2,2)*a(3,4)-a(3,2)*a(2,4))+
     $       a(1,2)*(a(2,1)*a(3,4)-a(3,1)*a(2,4))-
     $       a(1,4)*(a(2,1)*a(3,2)-a(3,1)*a(2,2))
c
c  Cofactors needed to calculate the S-wave transmission coeff.:
c
      c(1,4)=-a(2,1)*(a(3,2)*a(4,3)-a(4,2)*a(3,3))+
     $       a(2,2)*(a(3,1)*a(4,3)-a(4,1)*a(3,3))-
     $       a(2,3)*(a(3,1)*a(4,2)-a(4,1)*a(3,2))
      c(2,4)=a(1,1)*(a(3,2)*a(4,3)-a(4,2)*a(3,3))-
     $       a(1,2)*(a(3,1)*a(4,3)-a(4,1)*a(3,3))+
     $       a(1,3)*(a(3,1)*a(4,2)-a(4,1)*a(3,2))
      c(3,4)=-a(1,1)*(a(2,2)*a(4,3)-a(4,2)*a(2,3))+
     $       a(1,2)*(a(2,1)*a(4,3)-a(4,1)*a(2,3))-
```

```
     $       a(1,3)*(a(2,1)*a(4,2)-a(4,1)*a(2,2))
      c(4,4)=a(1,1)*(a(2,2)*a(3,3)-a(3,2)*a(3,3))-
     $       a(1,2)*(a(2,1)*a(3,3)-a(3,1)*a(2,3))+
     $       a(1,3)*(a(2,1)*a(3,2)-a(3,1)*a(2,2))
c
c  ..define the b vector for the incident P-wave case:
c
       b(1)=-a(1,1)
       b(2)=a(2,1)
       b(3)=-a(3,1)
       b(4)=a(4,1)
c
c  ..compute the P-P transmission coefficient:
c
       tpp=(b(1)*c(1,3)+b(2)*c(2,3)+b(3)*c(3,3)+b(4)*
     $c(4,3))/(a(1,1)*c(1,1)+a(2,1)*c(2,1)+a(3,1)*c(3,1)+
     $a(4,1)*c(4,1))
c
c  ..compute the P-SV transmission coeffient:
c
       tps=(b(1)*c(1,4)+b(2)*c(2,4)+b(3)*c(3,4)+b(4)*
     $c(4,4))/(a(1,1)*c(1,1)+a(2,1)*c(2,1)+a(3,1)*c(3,1)+
     $a(4,1)*c(4,1))
c
c  ..redefine b vector for the incident SV-wave case:
c
       b(1)=a(1,2)
       b(2)=-a(2,2)
       b(3)=a(3,2)
       b(4)=-a(4,2)
c
c  ..compute the SV-P transmission coefficient:
c
       tsp=(b(1)*c(1,3)+b(2)*c(2,3)+b(3)*c(3,3)+b(4)*
     $c(4,3))/(a(1,1)*c(1,1)+a(2,1)*c(2,1)+a(3,1)*c(3,1)+
     $a(4,1)*c(4,1))
c
c  ..compute the SV-SV transmission coefficient:
c
       tss=(b(1)*c(1,4)+b(2)*c(2,4)+b(3)*c(3,4)+b(4)*
     $c(4,4))/(a(1,1)*c(1,1)+a(2,1)*c(2,1)+a(3,1)*c(3,1)+
     $a(4,1)*c(4,1))
c
c  ..compute the SH-SH transmission coefficient:
c
       z1=dens*cs*cos(psi(ijk,1))
       z2=dens*cs*cos(psi(ijk,2))
       zsum=z1+z2
       tr=2.*z1*zsum/(zsum**2.+(w*z1*z2/stift)**2.)
       ti=2.*z1**2.*w*z2/stift/(zsum**2.+(w*z1*z2/stift)**2.)
       tsh=cmplx(tr,ti)
c
      return
      end
```

```
c
c
      subroutine stensor(j)
c
#include "common.f"
c
c  This subroutine sets up the Green's stress tensor.
c
      complex ep,es,cep,ces,sterm
c
      g12=gam(1)**2.
      g13=gam(1)**3.
      g22=gam(2)**2.
      g23=gam(2)**3.
      g32=gam(3)**2.
      g33=gam(3)**3.
      ep=cmplx(0.,w/cp*rrk(j))
      es=cmplx(0.,w/cs*rrk(j))
      cep=cexp(ep)/cp
      ces=cexp(es)/cs
      v=cs/cp
      v2=2.*v**2.
      diag=(1.-v2)
      sterm=cmplx(0.,w/4./pi/rrk(j))
c
c  .. compute P-wave Green's stress tensor:
      slmnp(1,1,1)=sterm*(diag*gam(1)+v2*g13)*cep
      slmnp(2,1,1)=sterm*v2*g12*gam(2)*cep
      slmnp(3,1,1)=sterm*v2*g12*gam(3)*cep
      slmnp(1,1,2)=sterm*(diag*gam(2)+v2*g12*gam(2))*cep
      slmnp(2,1,2)=sterm*v2*g22*gam(1)*cep
      slmnp(3,1,2)=sterm*v2*gam(1)*gam(2)*gam(3)*cep
      slmnp(1,1,3)=sterm*(diag*gam(3)+v2*g12*gam(3))*cep
      slmnp(2,1,3)=slmnp(3,1,2)
      slmnp(3,1,3)=sterm*v2*g32*gam(1)*cep
      slmnp(1,2,1)=slmnp(2,1,1)
      slmnp(2,2,1)=sterm*(diag*gam(1)+v2*g22*gam(1))*cep
      slmnp(3,2,1)=slmnp(3,1,2)
      slmnp(1,2,2)=slmnp(2,1,2)
      slmnp(2,2,2)=sterm*(diag*gam(2)+v2*g23)*cep
      slmnp(3,2,2)=sterm*v2*g22*gam(3)*cep
      slmnp(1,2,3)=slmnp(3,1,2)
      slmnp(2,2,3)=sterm*(diag*gam(3)+v2*g22*gam(3))*cep
      slmnp(3,2,3)=sterm*v2*g32*gam(2)*cep
      slmnp(1,3,1)=slmnp(3,1,1)
      slmnp(2,3,1)=slmnp(3,1,2)
      slmnp(3,3,1)=sterm*(diag*gam(1)+v2*g32*gam(1))*cep
      slmnp(1,3,2)=slmnp(3,1,2)
      slmnp(2,3,2)=slmnp(3,2,2)
      slmnp(3,3,2)=sterm*(diag*gam(2)+v2*g32*gam(2))*cep
      slmnp(1,3,3)=slmnp(3,1,3)
      slmnp(2,3,3)=slmnp(3,2,3)
      slmnp(3,3,3)=sterm*(diag*gam(3)+v2*g33)*cep
c
```

```
c  .. compute S-wave Green's stress tensor:
      slmns(1,1,1)=sterm*(2.*gam(1)-2.*g13)*ces
      slmns(2,1,1)=sterm*(gam(2)-2.*g12*gam(2))*ces
      slmns(3,1,1)=sterm*(gam(3)-2.*g12*gam(3))*ces
      slmns(1,1,2)=-sterm*2.*gam(2)*g12*ces
      slmns(2,1,2)=sterm*(gam(1)-2.*g22*gam(1))*ces
      slmns(3,1,2)=-sterm*2.*gam(1)*gam(2)*gam(3)*ces
      slmns(1,1,3)=-sterm*2.*g12*gam(3)*ces
      slmns(2,1,3)=slmns(3,1,2)
      slmns(3,1,3)=sterm*(gam(1)-2.*g32*gam(1))*ces
      slmns(1,2,1)=slmns(2,1,1)
      slmns(2,2,1)=-sterm*2.*g22*gam(1)*ces
      slmns(3,2,1)=slmns(3,1,2)
      slmns(1,2,2)=slmns(2,1,2)
      slmns(2,2,2)=sterm*(2.*gam(2)-2.*g23)*ces
      slmns(3,2,2)=sterm*(gam(3)-2.*g22*gam(3))*ces
      slmns(1,2,3)=slmns(3,1,2)
      slmns(2,2,3)=-sterm*2.*gam(3)*g22*ces
      slmns(3,2,3)=sterm*(gam(2)-2.*g32*gam(2))*ces
      slmns(1,3,1)=slmns(3,1,1)
      slmns(2,3,1)=slmns(3,1,2)
      slmns(3,3,1)=-sterm*2.*gam(1)*g32*ces
      slmns(1,3,2)=slmns(3,1,2)
      slmns(2,3,2)=slmns(3,2,2)
      slmns(3,3,2)=-sterm*2.*gam(2)*g32*ces
      slmns(1,3,3)=slmns(3,1,3)
      slmns(2,3,3)=slmns(3,2,3)
      slmns(3,3,3)=sterm*(2.*gam(3)-2.*g33)*ces
      return
      end
```

LAWRENCE BERKELEY LABORATORY
UNIVERSITY OF CALIFORNIA
INFORMATION RESOURCES DEPARTMENT
BERKELEY, CALIFORNIA 94720